*remote sensing*

MDPI

*Article*

# Comparison of the Spatial Characteristics of Four Remotely Sensed Leaf Area Index Products over China: Direct Validation and Relative Uncertainties

**Xinlu Li [1,2], Hui Lu [1,3,*], Le Yu [1,3] and Kun Yang [1,3,4]**

1 The Ministry of Education Key Laboratory for Earth System Modeling, Department of Earth System Science, Tsinghua University, Beijing 100084, China; xinlulee@outlook.com (X.L.); leyu@tsinghua.edu.cn (L.Y.); yangk@itpcas.ac.cn (K.Y.)
2 National Space Science Center, Chinese Academy of Science, Beijing 100190, China
3 The Joint Center for Global Change Studies, Beijing 100875, China
4 CAS Center for Excellence in Tibetan Plateau Earth Sciences, Beijing 100101, China
* Correspondence: luhui@tsinghua.edu.cn; Tel.: +86-010-62772565

Received: 21 November 2017; Accepted: 16 January 2018; Published: 22 January 2018

**Abstract:** Leaf area index (LAI) is a key input for many land surface models, ecological models, and yield prediction models. In order to make the model simulation and/or prediction more reliable and applicable, it is crucial to know the characteristics and uncertainties of remotely sensed LAI products before they are input into models. In this study, we conducted a comparison of four global remotely sensed LAI products—Global Land Surface Satellite (GLASS), Global LAI Product of Beijing Normal University (GLOBALBNU), Global LAI Map of Chinese Academy of Sciences (GLOBMAP), and Moderate-resolution Imaging Spectrometer (MODIS) LAI, while the former three products are newly developed by three Chinese research groups on the basis of the MODIS land reflectance product over China between 2001 and 2011. Direct validation by comparing the four products to ground LAI observations both globally and over China demonstrates that GLASS LAI shows the best performance, with $R^2$ = 0.70 and RMSE = 0.96 globally and $R^2$ = 0.94 and RMSE = 0.61 over China; MODIS performs worst ($R^2$ = 0.55, RMSE = 1.23 globally and $R^2$ = 0.03, RMSE = 2.12 over China), and GLOBALBNU and GLOBMAP performs moderately. Comparison of the four products shows that they are generally consistent with each other, giving the smallest spatial correlation coefficient of 0.7 and the relative standard deviation around the order of 0.3. Compared with MODIS LAI, GLOBALBNU LAI is the most similar, followed by GLASS LAI and GLOBMAP. Large differences mainly occur in southern regions of China. LAI difference analysis indicates that evergreen needleleaf forest (ENF), woody savannas (SAV) biome types and temperate dry hot summer, temperate warm summer dry winter and temperate hot summer no dry season climate types correspond to high standard deviation, while ENF and grassland (GRA) biome types and temperate warm summer dry winter and cold dry winter warm summer climate types are responsible for the large relative standard deviation of the four products. Our results indicate that although the three newly developed products have improved the accuracy of LAI estimates, much work remains to improve the LAI products especially in ENF, SAV, and GRA regions and temperate climate zones. Findings from our study can provide guidance to communities regarding the performance of different LAI products over mainland China.

**Keywords:** leaf area index; comparison; MODIS; uncertainty; China

## 1. Introduction

Leaf area index (LAI), defined as one-half of the total green leaf area per unit of ground horizontal surface area [1], is a key biophysical parameter in land surface processes and Earth system

models [2,3]. Global LAI products have been derived from satellites, which have the advantage of large spatial coverage and serve as inputs for many numerical models. For example, LAI is used in the European Centre for Medium-Range Weather Forecasts land surface model and has obvious impacts on simulation of carbon and water fluxes [4]. LAI is used to estimate the vegetation water content and then the contribution of vegetation layer to the microwave signals that could influence the performance of a land data assimilation system [5]. LAI is also the input of one-dimensional hydrology (1 dH) model for radiation flux estimation, particularly for estimation of transmissivity of shortwave radiation for canopy [6]. In addition, LAI is used as a parameter for estimating evapotranspiration based on some energy balance algorithms such as Two-Source Models (TSM) [7]. LAI can also be used in crop yield estimation system, and accurately assessing LAI is proven to be the key to improving estimation [8]. In order to effectively use LAI derived from remote sensing in various disciplines, it is critical to understand the characteristics and uncertainties of these products [9], because the quality, accuracy, and spatial–temporal coverage of these products still requires significant improvements [10].

With the development of remote sensing technology in the last few decades, remote sensors on board various satellite platforms have provided many LAI products of different spatial and temporal resolution at global or regional scales. For instance, GEOLAND (European FP6 project aiming at building up a European capacity for Global Monitoring of Environment and Security) LAI [11] is derived from SPOT/VEGETATION (The SPOT satellites are operated by the French Space Agency and Centre National d'Etudes Spatiales, and the VEGETATION instrument aims to provide accurate measurements of the main characteristics of the Earth's plant cover) with a 10-day time step and 1/112° (1 km at the equator) spatial resolution. The Moderate Resolution Imaging Spectroradiometer (MODIS) [12] on board the TERRA and AQUA satellites can provide global LAI in 1 km spatial resolution on four-day and eight-day time step LAI. GLASS LAI (Global Land Surface Satellites) is an improved LAI dataset based on MODIS reflectance data with eight-day temporal resolution and 0.05° (5 km at the equator) spatial resolution from 1981 to the present and 1 km spatial resolution from 2001 to the present [10]. GLOBALBNU LAI (GLOBAL LAI generated by Beijing Normal University) is a dataset that improved from MODIS LAI, with 1 km and eight-day resolution from 2000–2016 [13]. GLOBMAP LAI (GLOBal LAI MAP generated by Chinese Academy of Science) is another LAI dataset based on MODIS reflectance data, with 8 km and 16-day resolution from 1981–2000 and 500 m and eight-day resolution from 2001–2011 [14]. CYCLOPES (European Union FP5 project) LAI [15] is generated from the SPOT/VEGETATION sensor, with a 1/112° (1 km at the equator) spatial resolution and 10-day temporal resolution. GLOBCARBON (Europe Space Agency project intends to hone the accuracy of climate change forecasting) LAI [16] provides a monthly period and 1/11.2° (10 km at the equator) spatial resolution generated from a combination of SPOT/VEGETATION and ENVISAT/AATSR(Advanced Along Track Scanning Radiometer on board the European Space Agency's Envisat satellite) observations. ECOCLIMAP (National Center for Scientific Research program that provides a dual database at 1 km resolution that includes an ecosystem classification and a coherent set of land surface parameters that are primarily mandatory in meteorological modeling) LAI [17] obtained from NOAA/AVHRR (Advanced Very High Resolution Radiometer of National Oceanic and atmosphere administration) provides a one month and 1 km product. And CCRS (Canada Centre for Remote Sensing) LAI [18] is a regional LAI product that covers Canada based on the SPOT/VEGETATION sensor with 1 km and 10-day resolution. Land-SAF (Land Surface Analysis Satellite Applications Facility) LAI [19] is derived from the MSG/SEVIRI (Meteosat Second Generation Spinning Enhanced Visible and Infrared Imager) instrument over four specific regions (Europe, North Africa, South Africa and South America), with 3 km and daily resolution.

The uncertainty of LAI retrieval is easily influenced by atmosphere, sensor status and other factors [20]. In order to apply these products in various applications effectively, there is a great demand to validate their accuracy. Validation is the process of assessing by independent means the accuracy of data products [21]. At present, the method of validating LAI products can be divided into direct validation and comparison [22]. Direct validation involves directly assessing

the uncertainty of products through in situ measurements. For better direct validation, there is a need to consider the problem of spatial scale and to choose sites with homogeneous land cover. To achieve this goal, the committee on Earth Observation System-Land Product Validation (CEOS-LPV) organization generated an On Line Interactive Validation Exercise (OLIVE) platform [23], and some researches utilized this dataset to direct validate remote sensing land products including LAI [22,24]. Although they have made some progress, the existing validation datasets for direct validation are not representative of the global and seasonal variability of vegetation [24]. However, product comparison can achieve a spatial and temporal evaluation over a global and complete vegetation cycle, and can also provide the relative performance of each LAI retrieval algorithm [22]. Fang et al. [19] compared five major global moderate LAI products and analyzed the climatological and theoretical uncertainties. Zhu et al. [25] compared the FY-3A/MERSI (Medium Resolution Spectral Imager) LAI and MODIS LAI products over mainland China, and the results showed that both products could follow the growing season, but there are some disagreements due to different land cover types and terrain. Martin et al. [26] compared and evaluated the GIMMS LAI3g (Global Inventory Modeling and Mapping Studies three generation) and GGRS (Goettingen GIS & Remote Sensing) LAI products over Kazakhstan, and found pronounced LAI differences at both the start (spring) and end (fall) of the growing season.

The objective of this study was to compare and evaluate four global remotely sensed LAI products over China, namely GLASS (Global Land Surface Satellites) [10], GLOBALBNU (Global LAI Product of Beijing Normal University) [13], GLOBMAP (Global LAI Map of Chinese Academy of Sciences) [14], and MODIS LAI [27]. The first three are newly-released LAI products developed by Chinese groups and their performance has not been comprehensively evaluated. We used measured LAI from OLIVE and existing literature for direct validation [14]. The differences among the four products were also analyzed according to the Koppen–Geiger climate classification map and a land cover map. Such comparison and evaluation will help researchers with selecting LAI products, and in turn will help the producer to further improve the quality of their products. In the next section, we introduce the data and method used in this study. Section 3 presents the comparison results and evaluates performances; a discussion is presented in Section 3, and conclusions are given in Section 4.

## 2. Materials and Methods

### *2.1. GLASS LAI*

The GLASS LAI [10,28], available from http://glass-product.bnu.edu.cn/, is based on China's National High Technology Research and Development Program 863 key project 'Generation and application of global products of essential land variables'. A fused LAI dataset was generated from MODIS and CYCLOPES LAI products, and the MODIS and AVHRR surface reflectance was reprocessed to remove cloud and snow contamination. The training database was established over BELMANIP (Benchmark Land Multisite Analysis and Intercomparison of Products) sites, and then the general regression neural networks (GRNNs) were trained for each biome type to retrieve LAI from time-series reflectance data [29]. Then the entire year MODIS/AVHRR red and NIR reflectance data were input to the GRNNsto estimate one-year LAI pixel by pixel. In our study, we use the version 3 product. The product has different spatial resolutions at 5 km (about 0.05 degree at the equator) from 1981 to the present and 1 km after 2000, but the same time step of eight days for the whole temporal coverage.

### *2.2. GLOBALBNU LAI*

GLOBALBNU LAI dataset was generated by the Land-atmosphere Interaction Research Group of Beijing Normal University (GLOBALBNU LAI) with 1 km spatial resolution and eight-day time step from 2000–2016, distributed by http://globalchange.bnu.edu.cn/. It is an improved LAI dataset on the basis of MODIS LAI dataset through a two-step integrated method. First, the modified Temporal-Spatial Filter (mTSF) developed by TSF [30] was used to process the lower quality data

according to MODIS quality control (QC) and the data gaps and values were filled by making the best use of high-quality data. In the second step, the TIMESAT Savitzky–Golay (SG) filter was applied to post process the mTSF results to generate the final product [13]. The dataset is provided in NetCDF format with geographical coordinates.

### *2.3. GLOBMAP LAI*

The GLOBMAP LAI was generated as a consistent long-term global LAI product version 1 (1981–2011) by combining MODIS and historical AVHRR data, which can be downloaded from the website http://www.globalmapping.org/globalLAI/. MODIS series LAI data were derived from MODIS land surface reflectance and illumination and view angles data through a GLOBCARBON algorithm [31]. Then the relationship between AVHRR Simple Ratio (SR) and MODIS LAI was established pixel by pixel during the overlapped period 2000–2006. Following this the AVHRR LAI back to 1981 was estimated from AVHRR historical simple ratio index (SR) using these relationships [14]. The product is provided at 500 m spatial resolution and 8-day time step (2001–2011), and 16-day time step (1981–2000).

### *2.4. MODIS LAI*

The MODIS LAI can be derived from two satellites, TERRA and AQUA. Here we use TERRA MODIS Collection 5 product MOD15A2, available from https://ladsweb.nascom.nasa.gov/. The product was designed at 1 km spatial resolution and eight-day temporal resolution. The main algorithm was based on look-up-tables (LUTs) that estimated from a 3D radiation transfer model [27]. It compared MODIS directional spectral reflectance with model-based entries stored in LUTs and derived the distribution of all possible solutions [12]. In addition, the algorithm output is the mean LAI computed over the set of acceptable LUT elements for which simulated and measured MODIS surface reflectance differ within specified levels of model and surface reflectance uncertainties [22]. If the main algorithm failed, a back-up algorithm was employed that was based on the relationship between NDVI and LAI. A quality control (QC) layer was also provided to assess the retrieval quality.

Table 1 provides a summary of the four LAI products used in our study. According to Table 1, the overlapping period of four products is 2000–2011. Consequently, the comparison and evaluation work is focused on this period in this study.

**Table 1.** Main information on the LAI products under study.

| Product Name | Spatial Resolution | Temporal Resolution | Temporal Coverage |
|---|---|---|---|
| GLASS | 0.05°/1 km | 8 days | 1981–/2001– |
| GLOBALBNU | 1 km | 8 days | 2000–2016 |
| GLOBMAP | 8 km/500 m | 16 days/8 days | 1981–2000/2001–2011 |
| MODIS | 1 km | 8 days | 2000– |

### *2.5. Land Cover Map*

In order to compare the LAI differences among different biomes, the WestDC land cover map available from http://westdc.westgis.ac.cn was used (as Figure 1). It was produced based on the large-scale (1:100,000) land use database of China in 2000 made by Chinese Academy of Science [32]. The database was derived from Landsat MSS, TM, and ETM images, mainly by manual interpretation based on the experiences of experts and was validated by intensive field surveys. As found by Ran et al., WestDC land cover map has the highest accuracy over China and is employed as the reference map in the evaluation of land cover products over China [32].

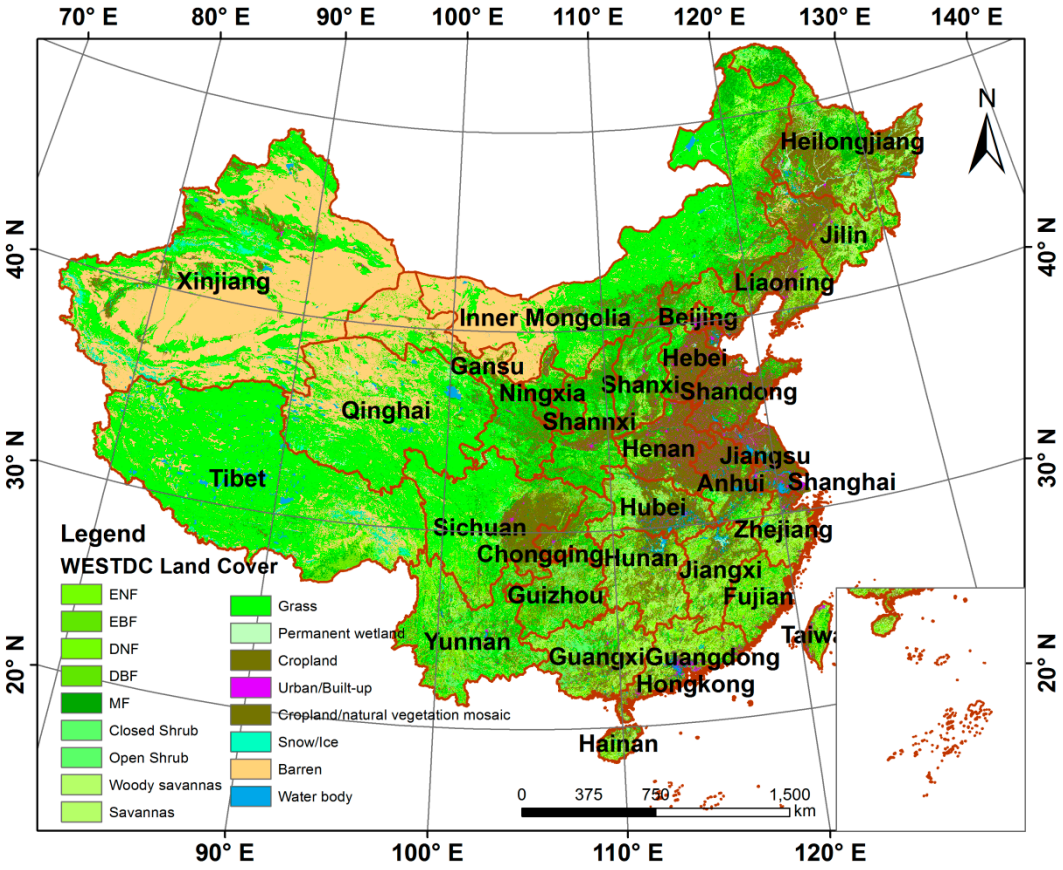


**Figure 1.** WestDC Land cover map over China. ENF represents evergreen needleleaf forest, EBF represents evergreen broadleaf forest, DNF represents deciduous needleleaf forest, DBF represents deciduous broadleaf forest, MF represents mixed forest.

### *2.6. Koppen–Geiger Climate Classification Map*

The differences of four LAI products were also analyzed by referring to the global climate map classifying through Koppen–Geiger system [33]. The Koppen–Geiger climate map is based on a large dataset of long-term monthly precipitation and temperature stations, using a two-dimensional thin-plate spline interpolation method. The map is divided into five first level climate types, as tropical (type A), arid (type B), temperate (type C), cold (type D), and polar (type E). The map has 0.1° spatial resolution, and can be downloaded from http://people.eng.unimelb.edu.au/mpeel/koppen.html. Figure 2 shows the Koppen–Geiger climate map of China, and Table 2 explains the meaning of the legend.

**Table 2.** The meaning of Koppen–Geiger climate classification.

| Climate | Meanings | Climate | Meanings |
|---|---|---|---|
| Am | Tropical zone monsoon | Cfb | Temperate zone warm summer; no dry season |
| Aw | Tropical zone savannah | Dsb | Cold zone dry summer; warm summer |
| BWk | Arid zone cold desert | Dsc | Cold zone dry summer; cold summer |
| BSh | Arid zone hot steppe | Dwa | Cold zone dry winter; hot summer |
| BSk | Arid zone cold steppe | Dwb | Cold zone dry winter; warm summer |
| CSb | Temperate zone dry warm summer | Dwc | Cold zone dry winter; cold summer |
| Cwa | Temperate zone dry hot summer | Dfa | Cold zone hot summer; no dry season |
| CWb | Temperate zone warm summer; dry winter | Dfb | Cold zone warm summer; no dry season |
| Cfa | Temperate zone hot summer; no dry season | ET | Polar zone tundra |

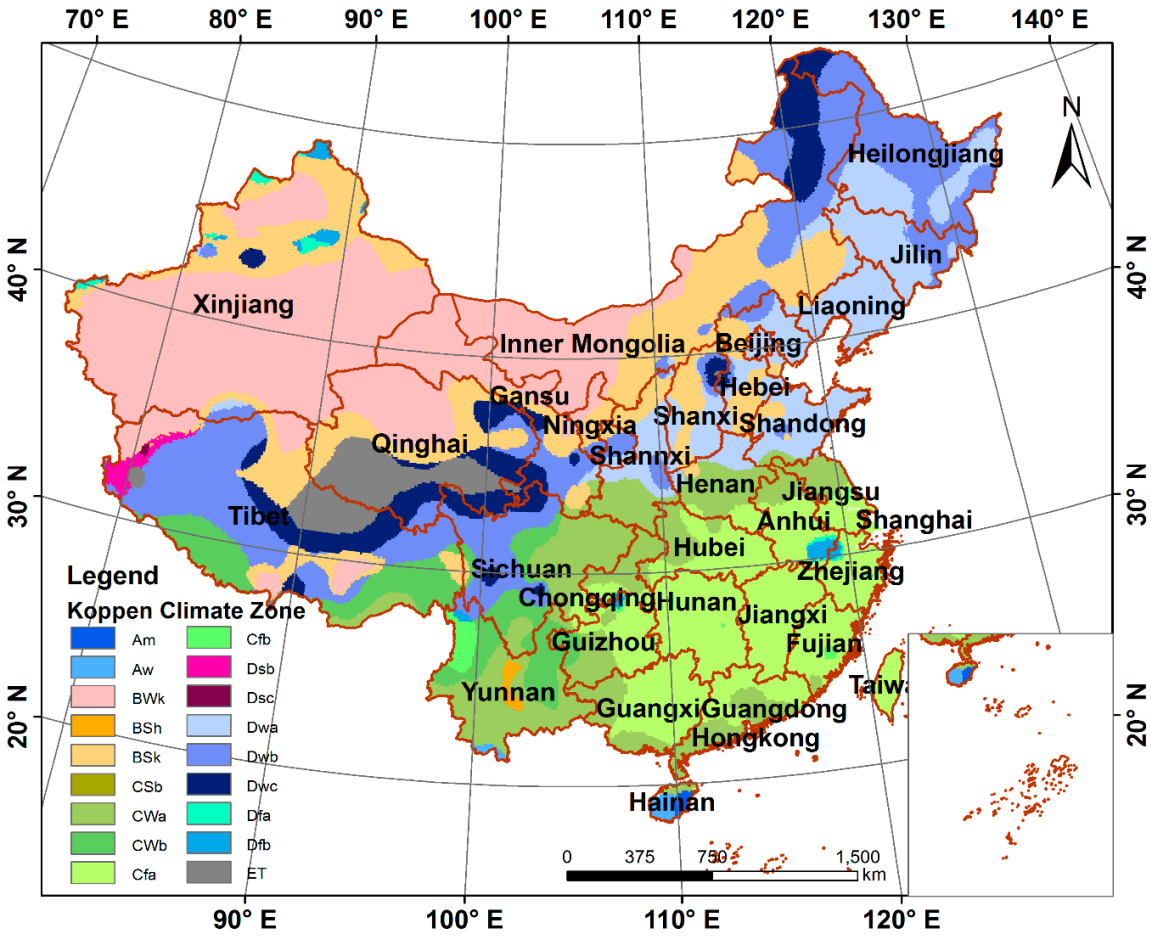


**Figure 2.** Koppen–Geiger climate classification over China.

### 2.7. Field Measured LAI

OLIVE (On Line Interactive Validation Exercise) platform is established by CEOS-LPV (Committee on Earth Observation System Land Product Validation) and it is devoted to the validation of global remotely sensed land surface products [23]. The OLIVE data has an independent database named DIRECT that include true LAI dataset that are all collected from the existing experimental networks such as FLUXNET, VALERI, Bigfoot, et al., whose sites are all selected at homogenous land cover types and can present 9–100 km$^2$ spatial range, and have also been utilized in other LAI product validation studies [22,24,29]. The dataset can be downloaded from http://calvalportal.ceos.org/web/olive/site-description. According to our study time range, we finally selected 47 field LAI measurements over 37 sites from the true LAI database with six biome types; one of them is located in China. And considering our study area, we also found another six field measurements located in China from the present literature [30]. They first established the empirical relationships between clear-sky TM/ETM+ image vegetation index such as NDVI (Normalized Difference Vegetation Index), SR (Simple Ratio), RSR (Reduced Simple Ratio), etc. and field measured LAI in the 30 × 30 m sampling plots, then generated fine-resolution LAI maps according to the relationships considering the foliage clumping and scale shift effect [13], and finally upscaled the 30 m LAI map to match with remote sensing LAI products [30]. Thus we have 53 field measurements in total, which include seven measurements in China. The distribution of global field measurement sites used for direct LAI validation is showed in Figure 3.

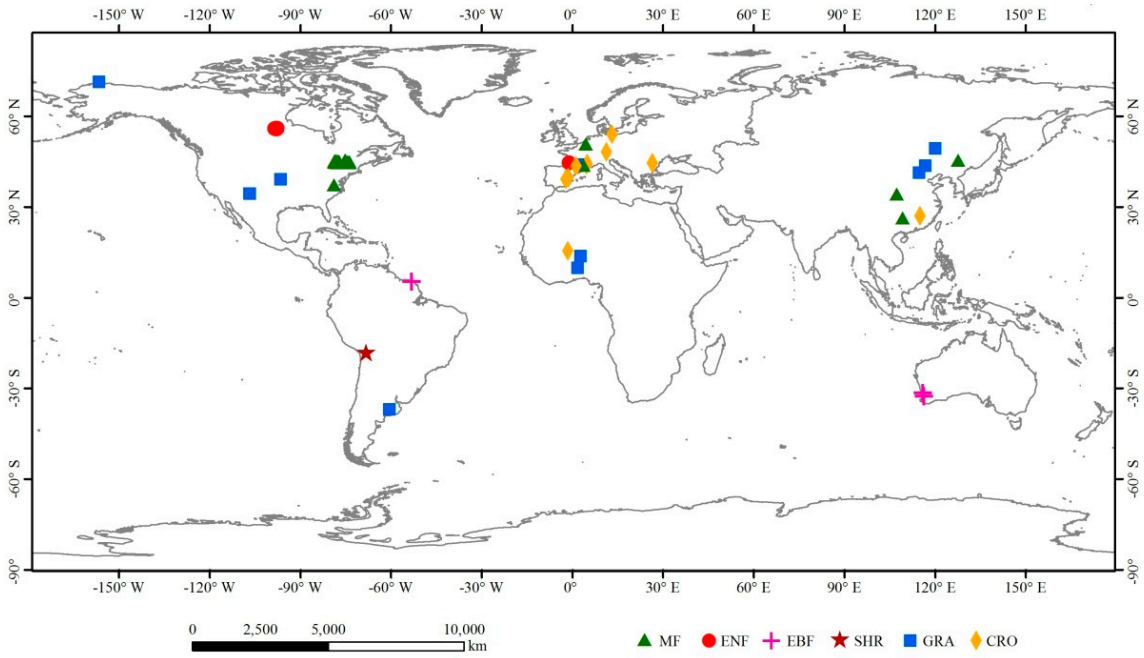


**Figure 3.** Distribution of field measurement LAI sites that are capable of direct LAI validation during 2001–2011.

### *2.8. Comparison Method*

The four products needed to be compared over the same spatial area and temporal period. In our study, we chose China as the study area because of its complex topography, various climate conditions and biome types; the three new LAI products were developed and maintained by Chinese groups and then expected to have reliable performance over China.

As stated in earlier research [22,24,29], direct validation is necessary to evaluate the accuracy of each product. Because the field measurements in China are too limited (only seven sites are available), we first validate the four products at global scale (53 measurement sits available), and then validate in China (seven measurement sites available). The results are shown in Section 3.1.

For LAI comparison, firstly, the four products were projected to the Albers projection coordinate system and resampled to 1 km by the nearest-neighbor sampling method for all the images during the overlapped period from 2001 to 2011. Then we calculated the yearly temporal mean LAI pixel by pixel for each year of each product as the basic data for comparison. The climatological LAI of each product was calculated by averaging the yearly temporal mean LAI from 2001 to 2011 and their spatial distribution was compared (Section 3.2.1). The difference among the four climatological LAI were presented in Section 3.2.2, while their spatial similarity was illustrated through scatter plots in Section 3.2.3. The standard deviation (SD) and relative standard deviation (RSD) were also analyzed in Section 3.2.4. SD and RSD are calculated as:

$$\mathrm{SD} = \sqrt{\frac{1}{N}\sum_{i=1}^{N}\left(LAI_i - \overline{LAI}\right)^2} \quad (1)$$

$$\mathrm{RSD} = \frac{SD}{\overline{LAI}} \quad (2)$$

where $LAI_i$ represents the four LAI product value, LAI is the mean of four products, and $N$ is the total number of products, in our study is 4.

Later, we computed the Pearson correlation coefficients (R) of the time series of yearly LAI pixel by pixel among four products and showed their spatial patterns in Section 3.3. R is computed as:

$$R = \frac{n\sum_{i=1}^{n} x_i y_i - \sum_{i=1}^{n} x_i \sum_{i=1}^{n} y_i}{\sqrt{n\sum_{i=1}^{n} x_i{}^2 - \left(\sum_{i=1}^{n} x_i\right)^2} \cdot \sqrt{n\sum_{i=1}^{n} y_i{}^2 - \left(\sum_{i=1}^{n} y_i\right)^2}} \quad (3)$$

where $x_i$, $y_i$ represent two time series LAI value respectively in this case, and $n$ represents the total number of year, which here is 11.

At last, we made the LAI difference case analysis, which included the mean SD/RSD and the LAI value difference for each biome type (Section 3.4.1), the proportion of each biome type at different SD/RSD significant levels and typical region case studies (Sections 3.4.2 and 3.4.3).

## 3. Results

### *3.1. Direct Validation with Field Measurement LAI*

We first validated the four LAI products: GLASS, GLOBALBNU, GLOBMAP, and MODIS to field measurement LAI. Considering the OLIVE sites are located in almost homogeneous land and the six China field measurements have been upscaled from high-resolution LAI images [30], we extracted the pixel value to directly match the field measurements. Furthermore, we chose images with the closest date to the ground measurement date for validation. Finally, we obtained 53 pixel LAI values for each LAI product for validation, and the uncertainty of each product was quantified by $R^2$, $p$-value, and RMSE. Table 3 summarizes the validation indictors of the four products for global with 53 sites and China with seven sites, respectively. For global validation, GLASS shows the highest accuracy ($R^2$ = 0.70, RMSE = 0.96). For direct validation over China, the lowest uncertainty was achieved by GLASS LAI ($R^2$ = 0.94, RMSE = 0.61), while the highest uncertainty was obtained by MODIS LAI ($R^2$ = 0.03, RMSE = 2.12).

**Table 3.** Validation indictors of four products.

| | Global | | | China | | |
|---|---|---|---|---|---|---|
| | $R^2$ | RMSE | $p$-Value | $R^2$ | RMSE | $p$-Value |
| GLASS | 0.70 | 0.96 | $6.62 \times 10^{-15}$ | 0.94 | 0.61 | $3.00 \times 10^{-4}$ |
| GLOBALBNU | 0.60 | 1.13 | $8.32 \times 10^{-12}$ | 0.52 | 1.06 | $6.79 \times 10^{-2}$ |
| GLOBMAP | 0.57 | 1.30 | $5.62 \times 10^{-11}$ | 0.77 | 1.15 | $9.00 \times 10^{-3}$ |
| MODIS | 0.55 | 1.23 | $2.82 \times 10^{-10}$ | 0.03 | 2.12 | $7.21 \times 10^{-1}$ |

Taking biome types into consideration, different LAI products have different performance. Figure 4 shows the validation scatter plots over global 53 sites. For grassland (GRA), shrubland (SHR) and cropland (CRO), GLASS, GLOBALBNU and MODIS LAI all perform well and the scatter plots mostly stand on the 1:1 line. For evergreen needleleaf forest (ENF), the four products all show two sites of them perform better, while the other two sites perform worse. For evergreen broadleaf forest (EBF), GLASS and MODIS perform best, followed by GLOBALBNU and GLOBMAP. For mixed forest (MF), the four products are all overestimated (green triangles in Figure 4).

Some possible uncertainty sources could attribute to the difference between remote sensing LAI and field-measured LAI. First is the inversion errors that resulted from difference between remote sensing observation reflectance and modeled reflectance. The observation reflectance could be affected by several factors such as aerosol, cloud contamination, topography, etc., while modeled reflectance could be affected by the calibration parameters, and they both accumulate errors during inversion processes. In addition, a vegetation reflectance saturation problem could affect inversion accuracy, that is, reflectance is insensitive to dense canopies LAI [18], and the large LAI uncertainty of evergreen needleleaf forest in Figure 4 (red dot) could be attributed to this.

Second is the field-measured errors. The field LAI measurements are obtained by LAI-2000, TRAC, etc. instruments, but they do not distinguish the effective photosynthetic tissue from non-photosynthetic tissues such as branches, stalks, and dead leaves, which could overestimate the LAI value [34]. The results in Figure 4 that remote sensing LAI is lower than field-measured LAI could be due to this reason. For some dense biomes, the field-measured LAI have not considered the underforest canopy, while remote sensing LAI is the observation of the vegetation vertical structure, which considers the underforest [35]. The overestimate of mixed forest in Figure 4 may result from this.

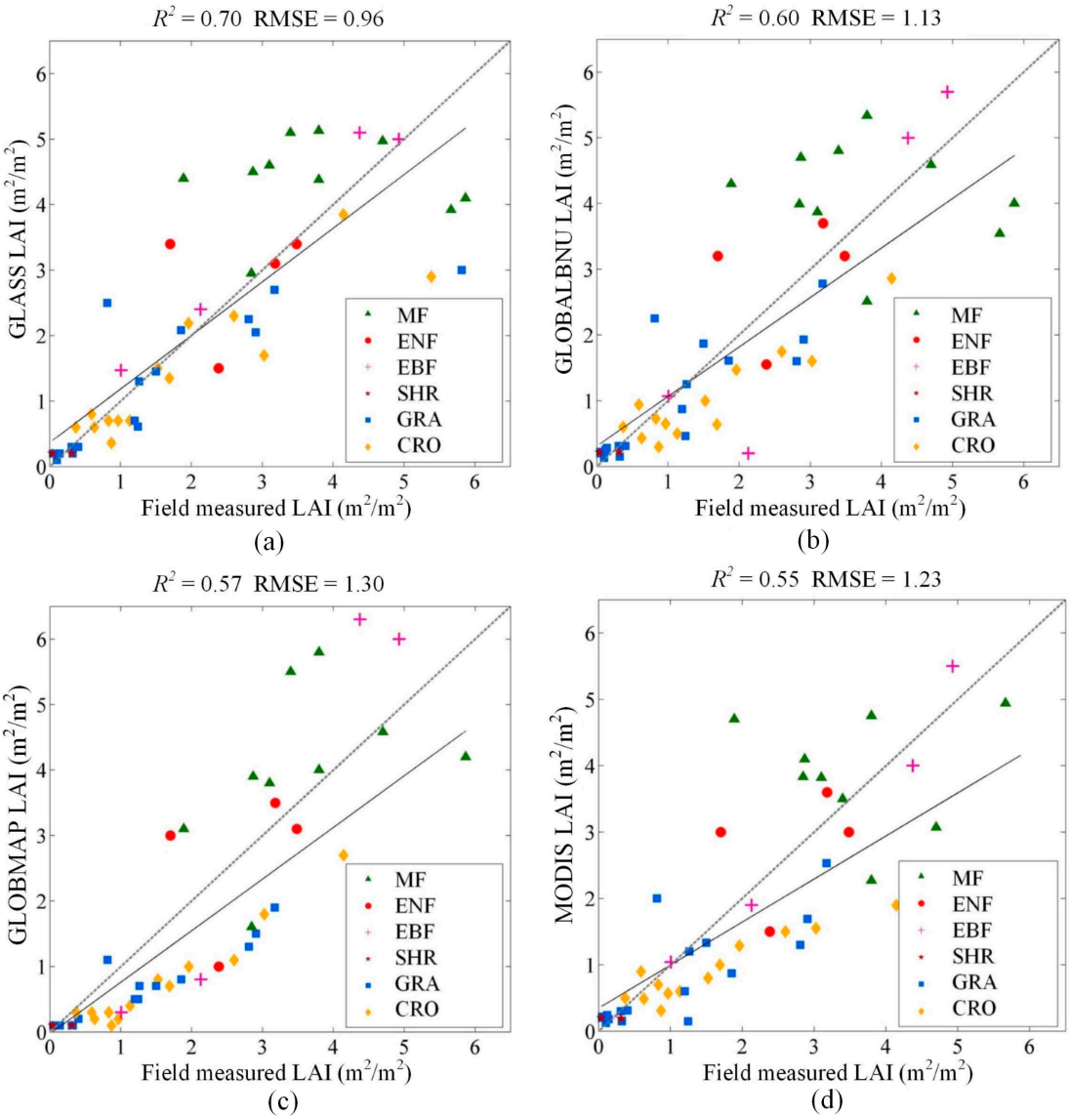


**Figure 4.** Directly validated scatter plots: (**a**) GLASS; (**b**) GLOBALBNU; (**c**) GLOBMAP; (**d**) MODIS. MF represents mixed forest, ENF represents evergreen needleleaf forest, EBF represents evergreen broadleaf forest, SHR represents shrubland, GRA represents grassland, CRO represents cropland.

Spatially, although most sites we chose are at homogenous land, but there are still some mixed land cover types and the scale effect is inevitable. Temporally, the TM/ETM+ images and field sampling date may be different during the generation process of fine-resolution LAI maps. In addition, the remote sensing LAI images are for dates closest to the field-measured dates. These are another two error sources that lead to validation uncertainty.

### *3.2. Spatial Characteristics of LAI Climatology Derived from Four Products*

#### 3.2.1. Spatial Distribution of Four LAI Climatologies

Figure 5 shows the spatial distribution of LAI climatology (11 years averaged LAI from 2001 to 2011) for each product. Generally, the four products are consistent in their patterns: a high LAI in the southeast and a low LAI in the northwest. Note that the pixels perennially at zero were set to null, which mainly occurs in the northwest of China. Considering the LAI values, four products show agreement in some regions: for example, in the northwest part of China (an arid or cold climate zone with mainly grassland land cover type), the LAI values are all in the range from 0 to 2. However, in the Sichuan basin in central China (red rectangles in Figure 5), with a cold climate and mainly covered with grassland in the west and a temperate climate and forest cover in the east, GLASS and GLOBMAP LAI mainly range from 2 to 4 at the edge of basin; GLOBALBNU LAI ranges from 0 to 2 in the western basin and 2 to 4 in the eastern basin, and MODIS LAI ranges from 0 to 2 in the whole basin. For southeast coastal regions located in a temperate climate and mainly covered with forest, GLOBMAP has a higher LAI than the other three products, while MODIS has the lowest LAI.

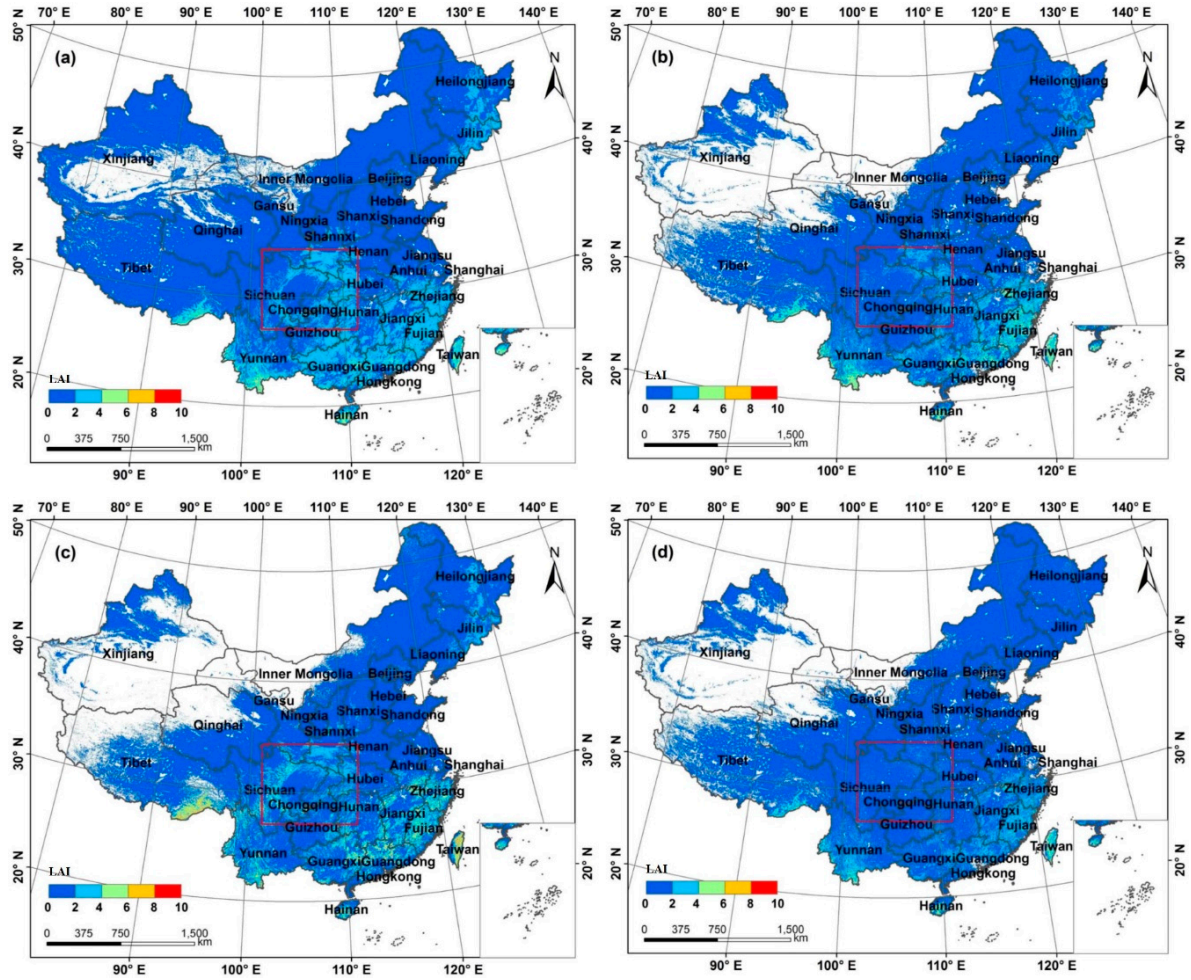


**Figure 5.** Spatial distributions of four LAI climatologies: (**a**) GLASS (**b**) GLOBALBNU; (**c**) GLOBMAP; (**d**) MODIS.

Figure 6 shows the boxplot of the overall LAI pixel values over China; the lines (from top to bottom) represent the maximum LAI value, 75% quartile value, median value, 25% quartile value, and minimum value, and the black spot represents the mean value. The results show that the four

products have the same minimum LAI, while the GLOBMAP product has the highest maximum value (9.25), followed by GLOBALBNU (6.20), MODIS (5.74), and GLASS (5.45). The mean values are almost the same for the four products (around 1.0), but GLOBMAP has the highest mean value (1.12). The interquartile range is lowest for MODIS (0.89), and the total spread is highest for GLOBMAP (9.25), which means GLOBMAP has the highest variation (1.19).

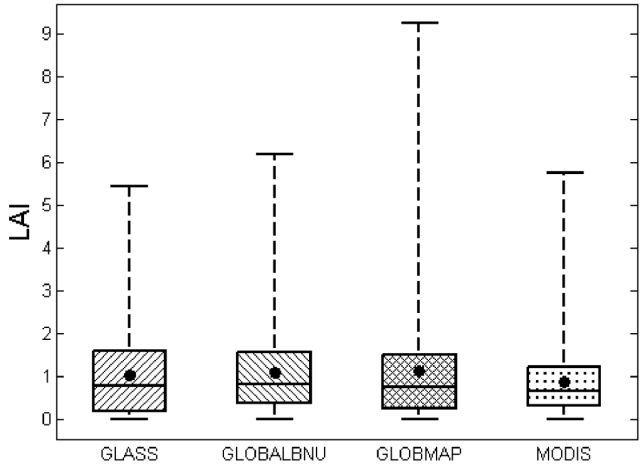


**Figure 6.** Boxplot of each LAI climatology. The lines (from top to bottom) represent the maximum LAI value, 75% quartile value, median value, 25% quartile value, and minimum value, respectively, and the black spot represents the mean value.

### 3.2.2. Spatial Differences of Four LAI Climatologies

Figure 7 demonstrates the differences between each pair of LAI products at the pixel scale. For all six pairs, most pixels show small differences (−1~1). However, large differences still exist in southern regions of China located in a temperate climate zone. The highest differences can reach over ±6 but this only occurs on a small proportion of pixels, and these mainly occur between GLOBMAP and MODIS (1149 pixels among total 6596588 pixels, 0.02%), and GLOBALBNU and GLOBMAP (376 pixels among total 6598208 pixels, 0.006%) products in southern Tibet with mixed forest (red rectangles in Figure 7c,f) and Taiwan with broadleaf and needleleaf forest (blue rectangles in Figure 7c,f). Among these six pairs, GLOBALBNU LAI and MODIS are the most similar (see Figure 7b). As shown in the histogram of Figure 8b, most of the different values are located in the −1 to 1 zone, but values from 0 to 1 are dominant (90%). This means GLOBALBNU is generally larger than MODIS. Eighty percent of the difference between GLASS and MODIS is positive (Figure 8a), but the difference between GLOBMAP and MODIS have half positive and half negative values, with some positive difference higher than 2 (Figure 8c). Most of the different pixels between GLASS and GLOBALBNU are located in the range of −2~2; 60% of the difference is positive while 40% is negative (Figure 8d). Eighty percent of the difference is positive between GLASS and GLOBMAP; between them, 75% of the pixels are located in the range of 0–1, and less than 5% of the pixels are located in the range of 1–2. For the rest of the 20% negative difference, about 15% are located in the range of −1~0, less than 5% are located in the range of −2~−1, and the others are in the range of less than −2 (Figure 8e). For GLOBALBNU and GLOBMAP, about 65% of the difference is positive and most of them are located in the range of 0–1. For the negative difference, about 30% are located in the range of −2~0; the other pixels are located in the range of −4~2 (Figure 8f).

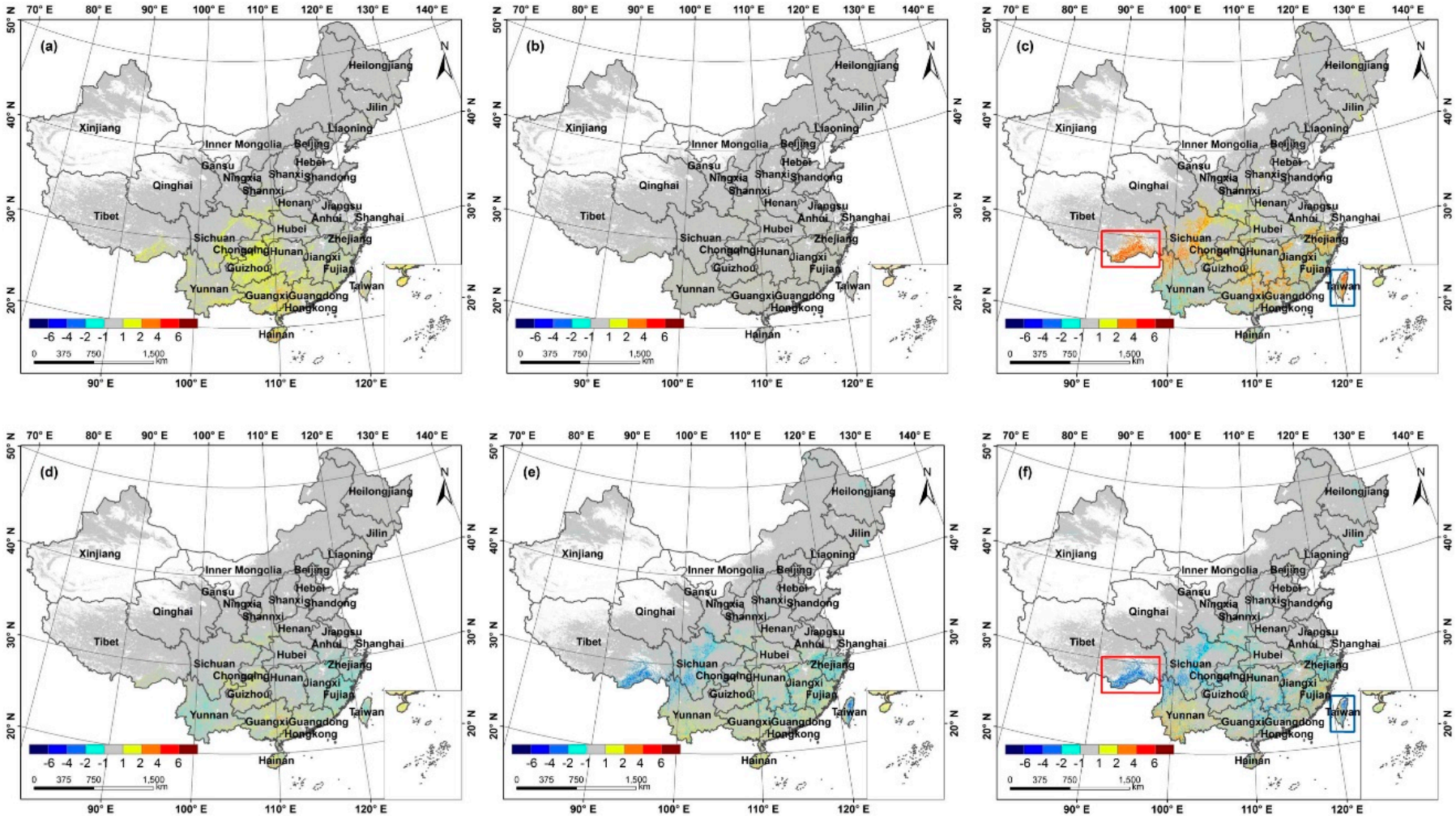


**Figure 7.** Spatial difference between each pairs of LAI products: (**a**) GLASS-MODIS; (**b**) GLOBALBNU-MODIS; (**c**) GLOBMAP-MODIS; (**d**) GLASS-GLOBALBNU; (**e**) GLASS-GLOBMAP; (**f**) GLOBALBNU-GLOBMAP.

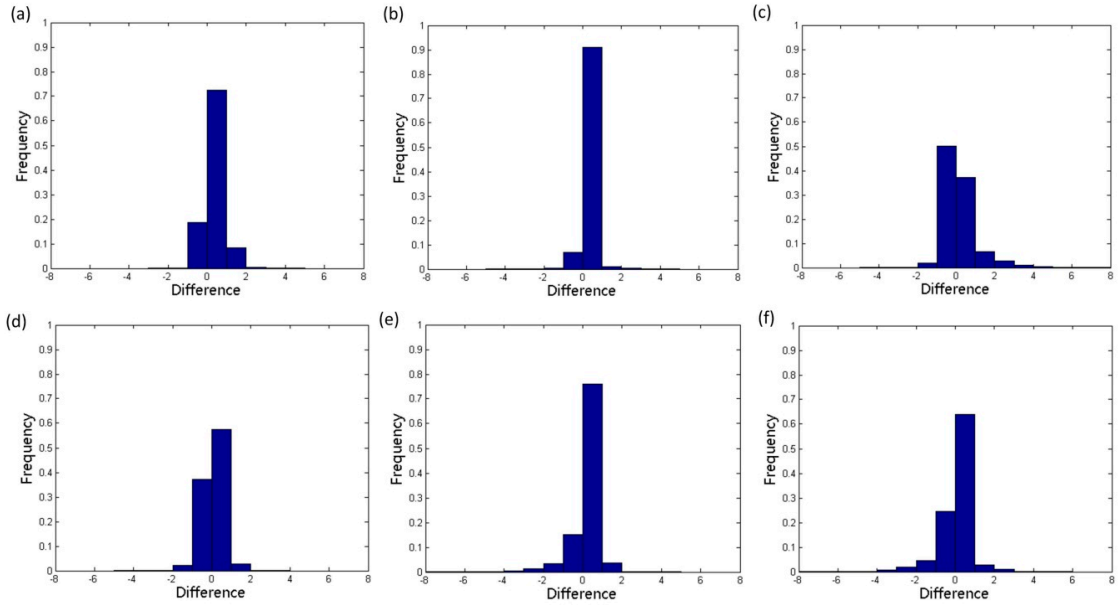


**Figure 8.** Frequency histograms of LAI differences: (**a**) GLASS vs. MODIS; (**b**) GLOBALBNU vs. MODIS; (**c**) GLOBMAP vs. MODIS; (**d**) GLASS vs. GLOBALBNU; (**e**) GLASS vs. GLOBMAP; (**f**) GLOBALBNU vs. GLOBMAP.

### 3.2.3. Spatial Correlation of Four LAI Climatologies

The spatial correlations among each pair of LAI products are shown in the density scatter plots in Figure 9. Different colors represent different levels of scatter numbers in each bin. As we can see from all six pairs, a greater density represents a larger concentration. And the densest values mainly occur with small LAI values. There are four pairs of the six have high correlation with $R^2 > 0.72$ (Figure 9a–e), and two pairs have moderate correlation with $R^2 = 0.58$ and 0.61, corresponding to GLOBMAP vs. MODIS and GLOBMAP vs. GLOBALBNU (Figure 9c,f). Compared with MODIS LAI, the correlation can be ordered by GLOBALBNU, GLASS, and CLOBMAP LAI.

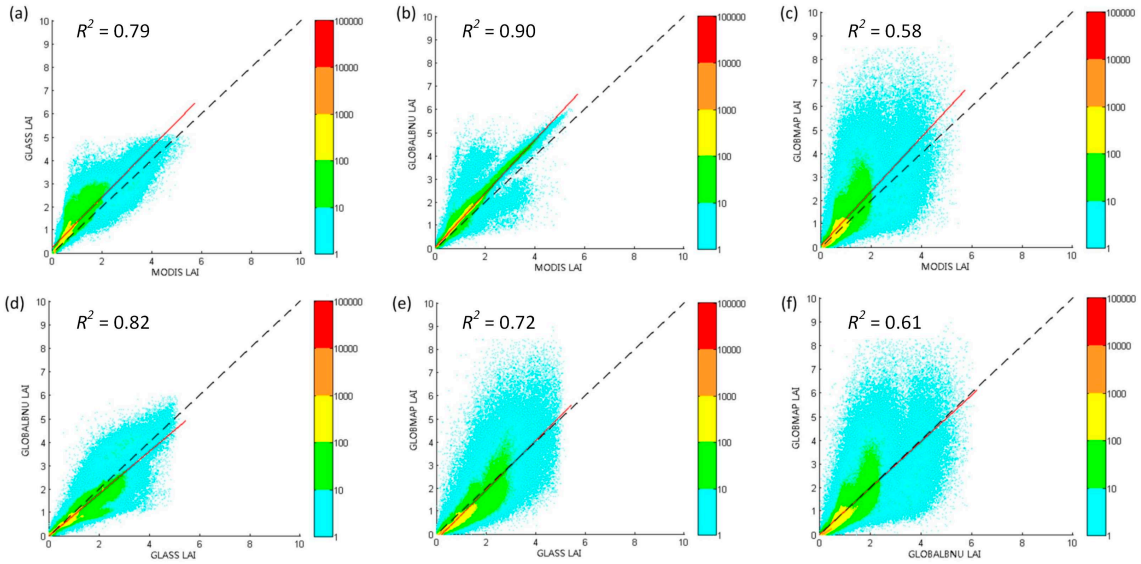


**Figure 9.** Density scatter plots of each pair of LAI products: (**a**) GLASS vs. MODIS; (**b**) GLOBALBNU vs. MODIS; (**c**) GLOBMAP vs. MODIS; (**d**) GLASS vs. GLOBALBNU; (**e**) GLASS vs. GLOBMAP; (**f**) GLOBALBNU vs. GLOBMAP.

3.2.4. Spatial Distribution of Standard Deviation (SD) and Relative Standard Deviation (RSD)

Figure 10 displays the standard deviation (SD) and relative standard deviation (RSD) among the four climatologies at the pixel level. From Figure 10a, we found a high discrepancy in southern China, while a small SD was mainly located in northern China (gray). Most of the high SD values are in the range of 0.5~1 and occur in southern regions, with values between 1 and 2 mainly occurring in southern regions in a temperate climate zone. Values between 2 and 3 mostly occur in southeast Tibet (red rectangle in Figure 10a) and Taiwan (blue polygon in Figure 10a) in temperate climate zones with mixed, broadleaf, and needleleaf forest. The largest SD, ranging from 3 to 4, is also distributed in the southeast of Tibet and Taiwan province, which is in line with former findings (Section 3.2.2).

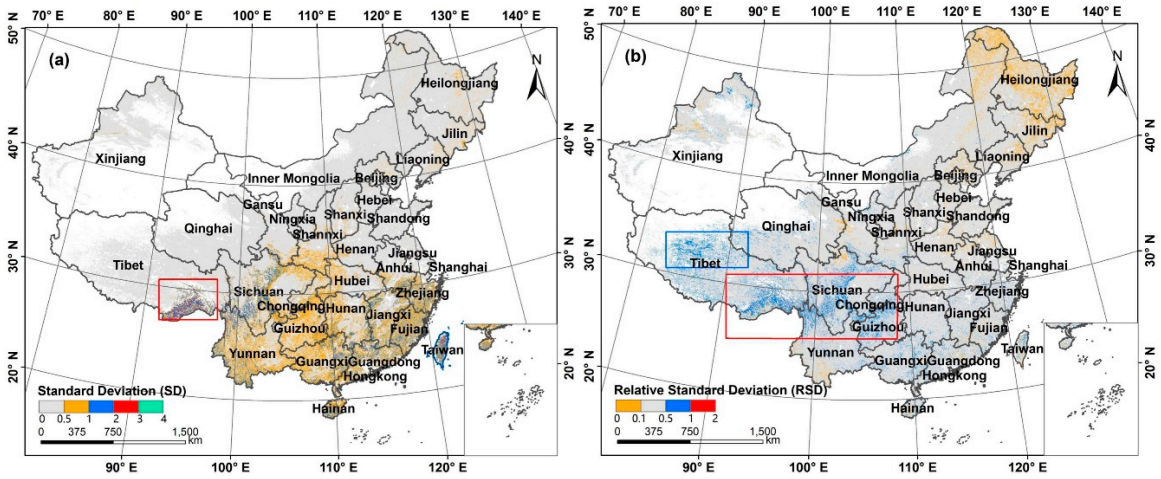


**Figure 10.** Standard deviation and relative standard deviation of the four products: (**a**) Standard deviation; (**b**) relative standard deviation.

However, in view of the fact that different biome types have different LAI magnitudes, the relative standard deviation (RSD) needs to be computed to eliminate the background effect, and the relative standard deviation (RSD) is standard deviation (SD) divided by mean LAI of the four products. In Figure 10b, we set four levels of relative standard deviation, being 0~0.1, 0.1~0.5, 0.5~1, and 1~2. For most of the pixels, the RSD are in the range of 0.1~0.5, which can be seen as an acceptable discrepancy (grey color). The lowest difference (0~0.1) pixels are mainly located in northeast China. The highest differences (0.5~2) occur in southern Tibet and Sichuan basin with mixed forest and grass land cover types, and northern Tibet in the biome ecotone of grassland and barren (blue and red rectangles in Figure 10b).

*3.3. Temporal Correlation of Time Series of Annual Mean LAI*

Figure 11 illustrates the temporal correlation among six pairs of annual mean LAI. For this 11-year time series, the correlation coefficients equal to ±0.48, ±0.55, and ±0.68 correspond to a 10%, 5%, and 1% significance level, respectively. For the six pairs, the significant correlation regions are mainly located in southern China (red color), which means the four products have high consistency in these regions. However, in most regions of southern China, we could not find a significant correlation (green). Specifically, GLOBALBNU and MODIS (Figure 11b) have a significant correlation in almost the whole of China, which reflects the temporal similarity of these two products.

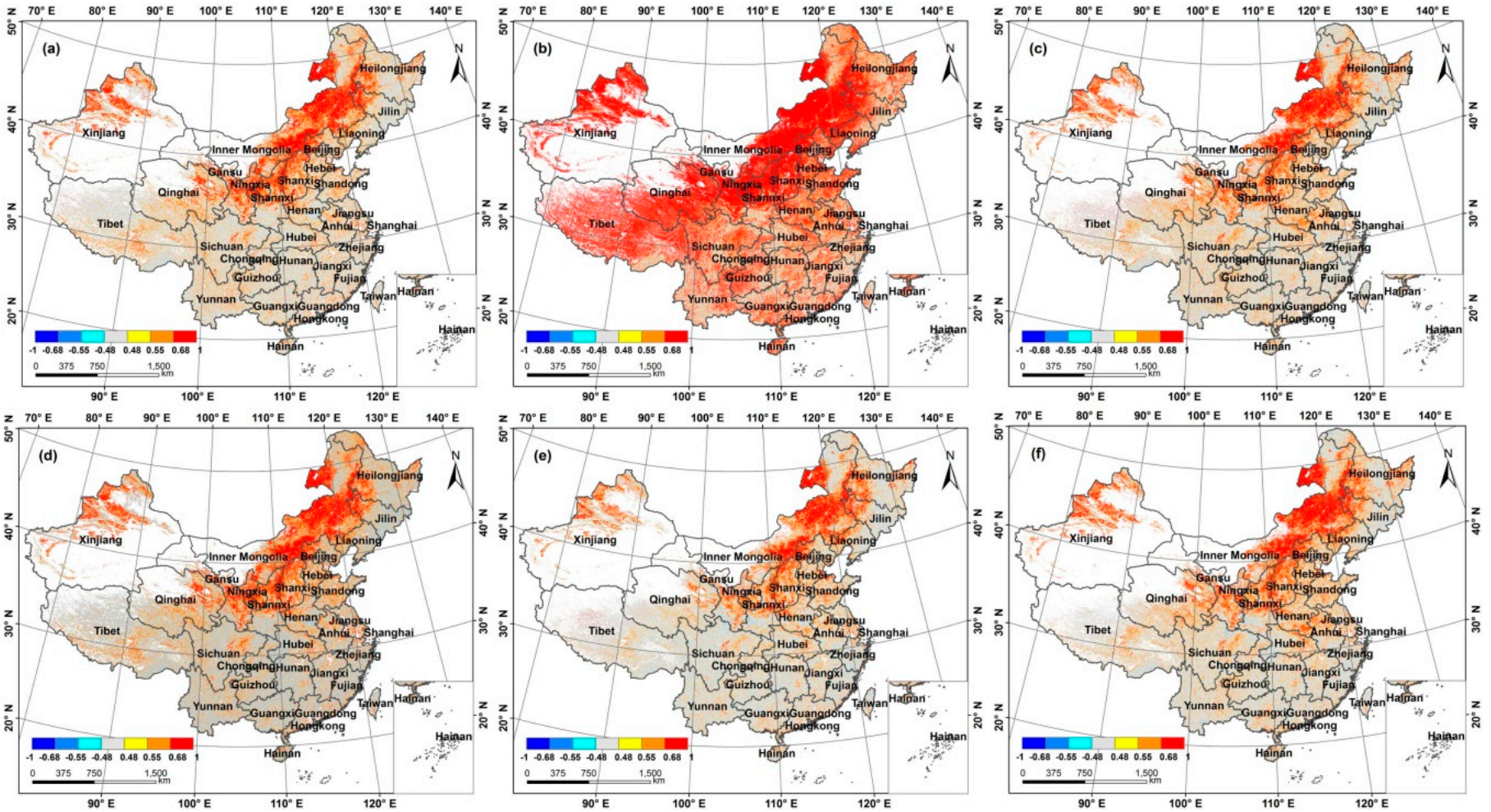


**Figure 11.** Temporal correlation among each pair of products: (**a**) GLASS vs. MODIS; (**b**) GLOBALBNU vs. MODIS; (**c**) GLOBMAP vs. MODIS; (**d**) GLASS vs. GLOBALBNU; (**e**) GLASS vs. GLOBMAP; (**f**) GLOBALBNU vs. GLOBMAP.

From the above analysis, we know the four LAI products have their own characteristics and differences. Although GLASS, GLOBALBNU, GLOBMAP, and MODIS LAI products are all inversed from MODIS land surface reflectance product MOD09, differences still exist among these four LAI products, which can be caused by several key factors. First is the process of input land surface reflectance. Although the product has been atmospherically corrected, there still exists some residual contamination such as aerosol, cloud, snow, etc. In view of this, GLASS LAI has produced a 500-m cloud and snow mask to reprocess the MOD09 product according to a method proposed by Tang [36]. GLOBALBNU LAI maintains the pixels of MODIS QC = 0, which means pixels with no cloud and snow, and makes a two-step spatial and temporal filter for pixels QC > 0. GLOBMAP was filtered by MOD09 cloud mask layer, and MODIS adopted a back-up algorithm when the main algorithm failed because of cloud contamination.

The second factor is the LAI retrieval algorithm. There are two main methods to retrieve LAI. One is empirical and is based on the relationship between LAI and VI. The other is a physical method that relies on the reversion of a canopy radiative transfer model, such as the MODIS look-up-table method and artificial neural networks [29]. GLASS LAI uses general regression neural networks to generate a yearly LAI product from time series MODIS reflectance, which belongs to a physical method. GLOBMAP integrates MODIS reflectance and the GLOBCARON algorithm to retrieve improved LAI from 2000 to 2011. To retrieve LAI back to 1981, a pixel-by-pixel relationship is established between improved LAI and AVHRR NDVI, which is an empirical method. MODIS LAI employs look-up tables simulated from a 3D radiative transfer model, and GLOBALBNU LAI filters the MODIS LAI. These are both physical methods.

The third factor can be attributed to land cover maps. In these four LAI retrieval systems, four different land cover inputs are used. GLASS classifies the biome into eight types according to the MCD12Q1 type 3 layer (grass and cereal crop, shrub, broadleaf crop, savanna, evergreen broadleaf, deciduous broadleaf, evergreen needleleaf, deciduous needleleaf). GLOBALBNU LAI uses the MCD12Q1 type 5 layer, without cereal crop and savanna but with increased barren and sparse vegetation type. GLOBMAP LAI uses the MCD12Q1 type 1 layer, which classifies the biome into six types, including grass and cereal crop, conifer forest, tropical forest, deciduous forest, mixed forest, and shrub, and MODIS classifies biome into grass and cereal crop, shrub, broadleaf crop, savanna, broadleaf forest, and needleleaf forest, and separates cereal crops and broadleaf crops. Myneni et al. [12] estimated that classification errors in land cover maps can generate an LAI estimation error of up to 50%, thus land cover types in an LAI retrieval system play an important role and should not be neglected.

Other factors can be related to a clumping index. For field measurement of LAI data, different measurement methods can lead to different LAI. For instance, LAI derived by direct and destructive measurement can be considered true LAI, while indirect methods such as LAI2000 instrument can be regarded as effective LAI. The distinction between true LAI and effective LAI is whether the measurements take the foliage's spatial distribution into account, for we assume the plant canopy architecture is under random distribution. The clumping index is the measure of foliage grouping relative to a random distribution of leaves in space [37], which provides the conversion between effective and true LAI. However, the four LAI products used in our study adopt different clumping indexes. GLASS LAI uses a clumping index map derived from POLDER 3 [38], which has removed the topographical effect that leads to a cross-biome difference [24], while GLOBALBNU and GLOBMAP LAI uses the POLDER 1 clumping index developed by Chen [39].

### *3.4. LAI Difference Case Analysis*

#### 3.4.1. LAI Performance of Different Biome Types and Climate Zones

We then studied the LAI performance for each biome type and climate zone. According to the WestDC land cover classification system, we selected all the vegetation types and merged similar types.

For instance, shrubs and open shrubs were merged into shrub, and we regarded woody savannas and savannas as savannas. Finally, we selected nine biome types for further study. According to the Koppen climate classification system, we listed 18 climate zones in China for analysis. Table 4 shows the mean SD and RSD for each biome type and Table 5 shows the similar climate zone results.

**Table 4.** Mean SD and RSD for each biome type.

| Biome Type | Sample Size (%) | Mean SD | Mean RSD |
|---|---|---|---|
| ENF | 278,710 (3.96) | 0.72 | 0.33 |
| EBF | 61,234 (0.87) | 0.75 | 0.27 |
| DNF | 21,814 (0.31) | 0.23 | 0.17 |
| DBF | 109,151 (1.55) | 0.52 | 0.24 |
| MF | 254,377 (3.61) | 0.46 | 0.23 |
| SHR | 509,575 (7.23) | 0.45 | 0.30 |
| SAV | 889,432 (12.62) | 0.54 | 0.27 |
| GRA | 3,036,273 (43.09) | 0.17 | 0.30 |
| CRO | 1,885,590 (26.76) | 0.26 | 0.26 |

**Table 5.** Mean SD and RSD for each climate zone.

| Climate Zone | Sample Size (%) | Mean SD | Mean RSD |
|---|---|---|---|
| Tropical zone monsoon | 8444 (0.13) | 0.74 | 0.32 |
| Tropical zone savannah | 20,613 (0.32) | 0.80 | 0.28 |
| Arid zone cold desert | 201,247 (3.10) | 0.09 | 0.33 |
| Arid zone hot steppe | 15,395 (0.24) | 0.55 | 0.30 |
| Arid zone cold steppe | 990,009 (15.23) | 0.10 | 0.29 |
| Temperate zone dry warm summer | 144 (0.002) | 0.44 | 0.31 |
| Temperate zone dry hot summer | 997,948 (15.36) | 0.49 | 0.29 |
| Temperate zone warm summer; dry winter | 355,910 (5.48) | 0.48 | 0.38 |
| Temperate zone hot summer; no dry season | 1,201,864 (18.49) | 0.55 | 0.29 |
| Temperate zone warm summer; no dry season | 39,920 (0.61) | 0.71 | 0.37 |
| Cold zone dry winter; warm summer | 460 (0.01) | 0.05 | 0.47 |
| Cold zone dry winter; cold summer | 47 (0.001) | 0.06 | 0.60 |
| Cold zone dry winter; hot summer | 844,135 (12.99) | 0.19 | 0.24 |
| Cold zone dry winter; warm summer | 1,086,738 (16.72) | 0.19 | 0.25 |
| Cold zone dry winter; cold summer | 446,007 (6.86) | 0.17 | 0.24 |
| Cold zone hot summer; no dry season | 19,178 (0.30) | 0.24 | 0.27 |
| Cold zone warm summer; no dry season | 37,237 (0.57) | 0.48 | 0.31 |
| Polar zone tundra | 233,782 (3.60) | 0.09 | 0.32 |

For biome types (Table 4), the result of mean SD shows that evergreen broad forest (EBF), evergreen needleleaf forest (ENF), and savanna (SAV) have the highest difference, with mean SD of 0.75, 0.72, and 0.54, respectively; while grassland (GRA), deciduous needleleaf forest (DNF), and cropland (CRO) have the lowest mean SD, with mean SD of 0.17, 0.23, and 0.26 respectively. When considering mean RSD, the highest discrepancy occurs in evergreen needleleaf forest (ENF), shrub (SHR), and savanna (GRA), while the lowest difference occurs in deciduous needleleaf forest (DNF), deciduous broadleaf forest (DBF), mixed forest (MF), and cropland (CRO). One thing worth mentioning in Table 4 is that the RSD for almost all biomes is on the order of 0.3, which indicates a typical 30% uncertainty for LAI products.

For climate zones (Table 5), tropical savannah, tropical monsoon, and temperate warm summer no dry season climate show the highest mean SD; the values are 0.80, 0.74, and 0.71. Cold dry cold summer, cold dry warm summer, arid cold desert, and polar tundra show the lowest SD with values of 0.05, 0.06, 0.09, and 0.09. From the perspective of RSD, cold zone dry and cold summer, cold zone dry and warm summer and temperate warm summer/dry winter climate show the highest RSD (values of 0.60, 0.47, and 0.38), while cold dry winter/hot summer, cold dry winter/warm summer, and cold dry

winter/cold summer show the lowest RSD, with values of 0.25, 0.24, and 0.24. From Table 5, it is also confirmed that, for most climate zones, the RSD is on the order of 0.3 and in line with the findings from biome types.

Figure 12 shows the bar plots of spatial average LAI differences for each biome type. Compared with MODIS LAI, the other three products all have positive bias for all biome types (Figure 12a–c). It means the three newly developed LAI datasets have larger values than their basis for all land cover types. For GLASS LAI, six of the nine biome types have a difference higher than 0.4: cropland is nearly 0.4, DNF is 0.2, and grassland has the lowest difference with less than 0.1. For GLOBALBNU, the differences of most types are 0.4, DNF and cropland are 0.2, and grassland is also the lowest (less than 0.1). For GLOBMAP, ENF shows the highest difference (more than 1), and grassland and cropland have the lowest difference (less than 0.1). For GLASS and GLOBALBNU (Figure 12d), DNF and grassland are almost the same; differences of the other types are 0.2 or so. For GLASS and GLOBMAP (Figure 12e), cropland has a large positive difference while ENF has a large negative difference, and grassland, savannas, and EBF have the lowest difference. For GLOBALBNU and GLOBMAP (Figure 12f), most of the differences are negative, the highest difference of which occurs in ENF. This means both GLASS and GLOBMAP have larger values than GLOBALBNU for most biome types.

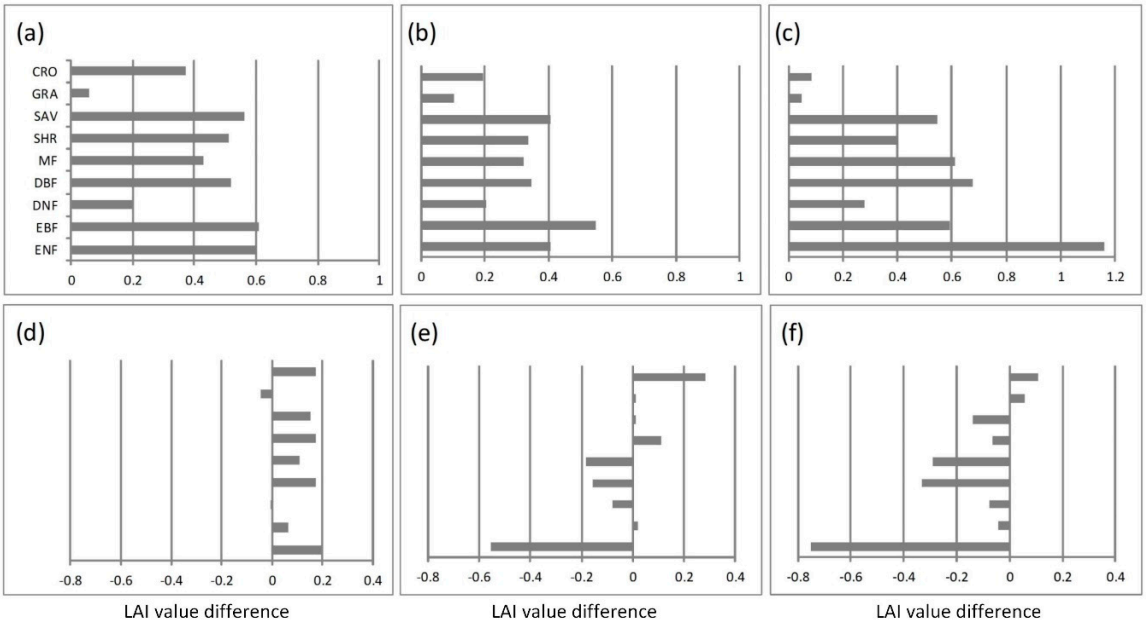


**Figure 12.** LAI value difference between LAI climatologies for each biome type: (**a**) GLASS-MODIS; (**b**) GLOBALBNU-MODIS; (**c**) GLOBMAP-MODIS; (**d**) GLASS-GLOBALBNU; (**e**) GLASS-GLOBMAP; (**f**) GLOBALBNU-GLOBMAP. ENF represents evergreen needleleaf forest, EBF represents evergreen broadleaf forest, DNF represents deciduous needleleaf forest, DBF represents deciduous broadleaf forest, MF represents mixed forest, SHR represents shrubland, SAV represents savannas, GRA represents grassland, and CRO represents cropland).

Figure 13 illustrates LAI difference between six pairs of LAI products for each climate type. GLASS has a more positive bias than MODIS for almost all climate types except Dsc and Dsb, and most of the difference values are in the range of 0–1 (Figure 13a). GLOBALBNU has a positive bias compared with MODIS for all climate types, and the difference values are relatively low (within 0.5 or so) (Figure 13b). For GLOBMAP, the LAI difference values for 11 out of 18 climate types have a positive bias, and seven have a relatively low negative bias (within −0.3 or so): Bwk, Bsh, Bsk, Csb, Dsb, Dsc, and ET. Comparing Figures 12 and 13, it can be found that GLOBALBNU has larger values than MODIS for all biome types and climate zones.

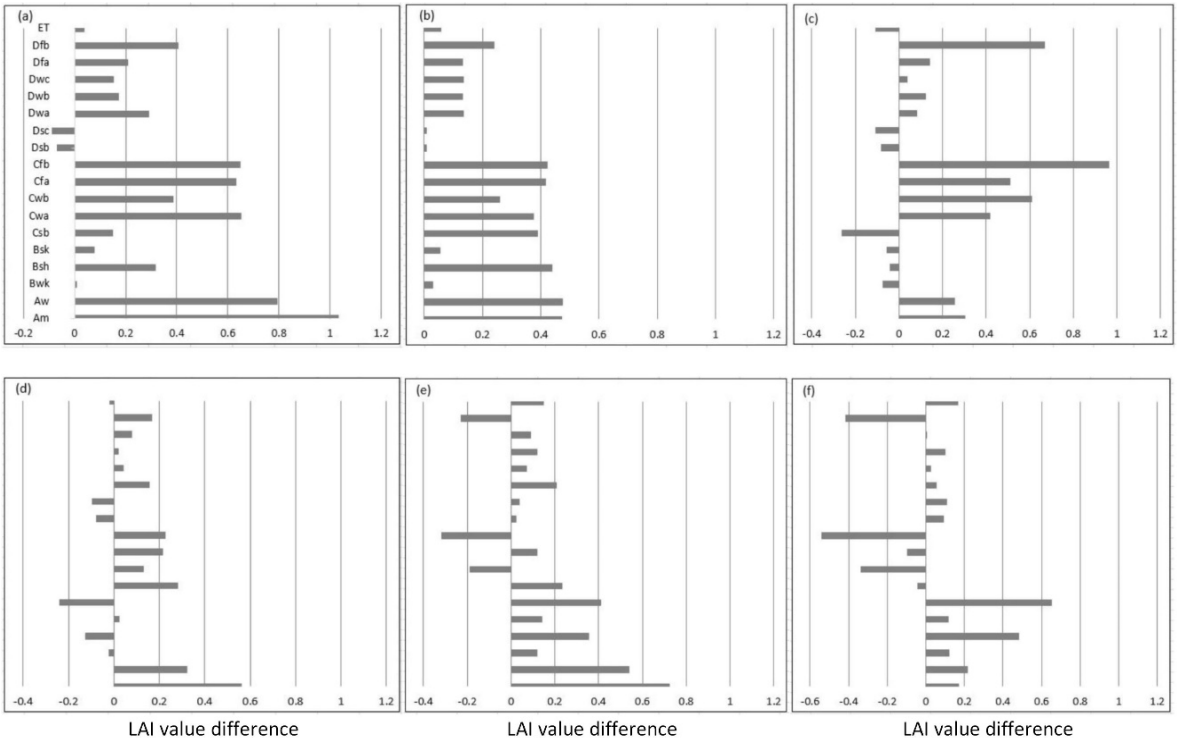


**Figure 13.** LAI value comparison for each climate type: (**a**) GLASS-MODIS; (**b**) GLOBALBNU-MODIS; (**c**) GLOBMAP-MODIS; (**d**) GLASS-GLOBALBNU; (**e**) GLASS-GLOBMAP; (**f**) GLOBALBNU-GLOBMAP.

Compared with GLOBALBNU, GLASS has a positive bias within 0.3 for 12 climate types, and negative bias for the other six climate types (Figure 13d). Compared with GLOBMAP, GLASS has a positive bias for 15 climate types and most of the bias is within 0.4, while there is a negative bias for the other three climate types (Figure 13e). Compared with GLOBMAP, GLOBALBNU has a positive bias within 0.6 for 13 climate types, and negative bias within −0.6 for the other five climate types.

### 3.4.2. Standard Deviation (SD)

To analyze the significance of the inconsistencies between the four products, we first computed the 90%, 95%, and 99% percentile of standard deviation (Figure 14). The 99% percentile SD (red color) mainly occurs in southern Tibet (Region A in Figure 14), western Sichuan with mixed forest and grass land cover types (region B in Figure 14), and Taiwan (region C in Figure 14) with mainly broadleaf and needleleaf forest; the 95% percentile SD (green color) mostly occurs in southern provinces in temperate climate zones with mixed forest and savannas biomes, and 90% percentile SD (blue color) mainly occurs in eastern Sichuan province in a cold climate zone with mainly grass.

We extracted three 99% percentile SD typical regions according to pixel density and geographic location (Tibet, Sichuan, and Taiwan (regions A, B, and C)), then calculated the minimum, maximum, median, mean, 25% and 75% quartile values for each product and the boxplots (Figure 15). Because GLASS LAI performs best in direct validation, we set GLASS LAI as the benchmark. For the Tibetan region (region A), the main reason for the difference could be due to GLOBMAP LAI, whose mean value is quite high compared with the other three products. For the Sichuan region (region B), the main reason for the difference can also be attributed to GLOBMAP and MODIS LAI, as the mean GLOBMAP LAI is a little high while MODIS LAI is a little low with an LAI difference of 0.5 $m^2/m^2$ between them. Also, for the Taiwan region (region C), the difference may be because of the high deviation of GLOBMAP.

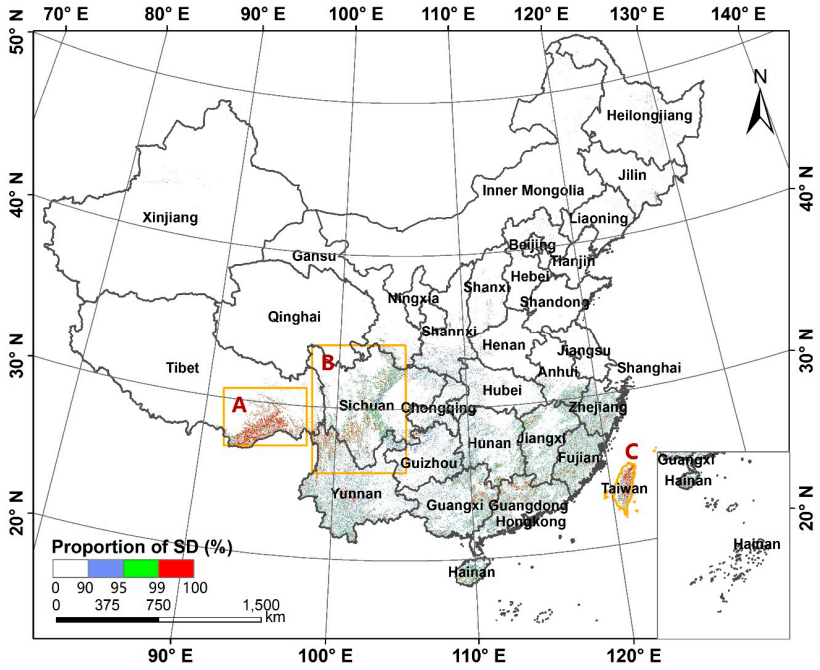


**Figure 14.** Percentile distribution of standard deviation of four LAI climatologies over China. Blue represents 90% percentile level, green represents 95% percentile level, and red represents 99% percentile level.

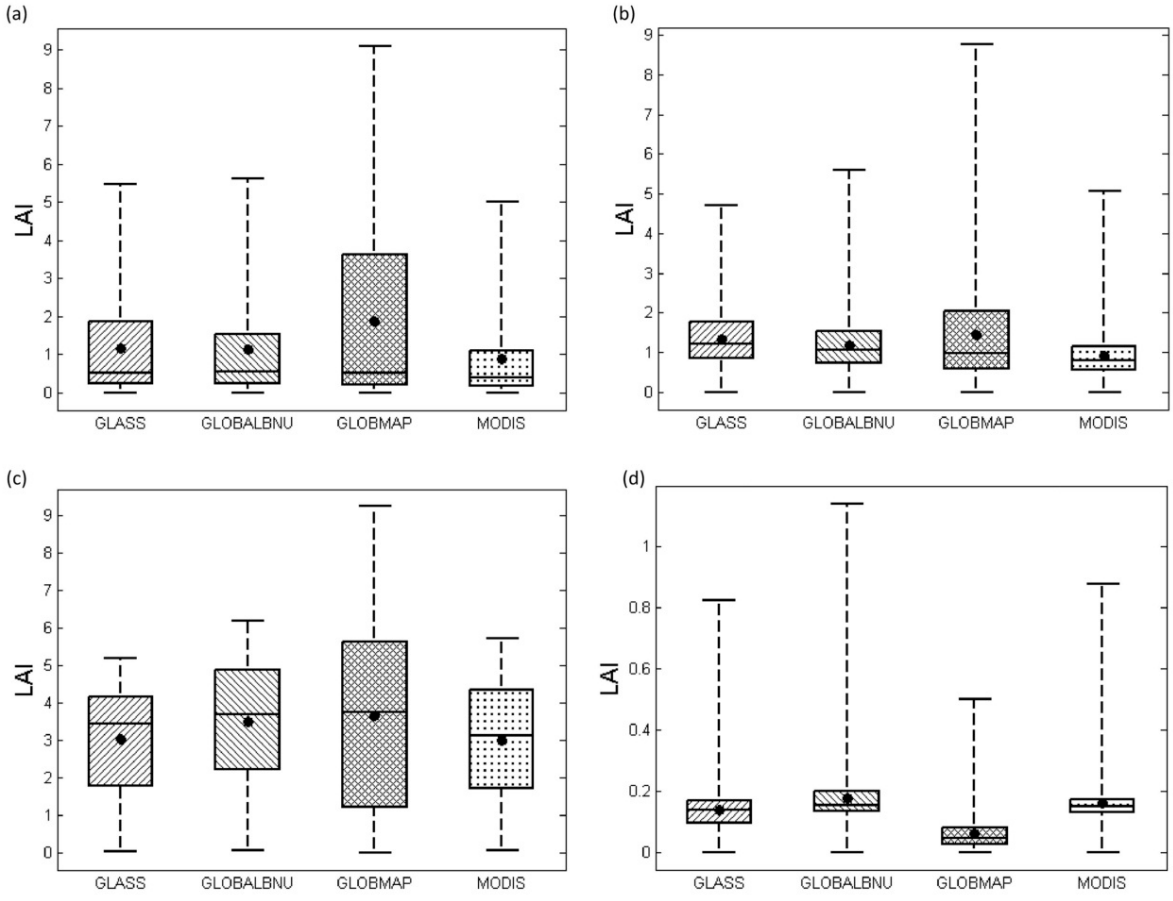


**Figure 15.** LAI boxplots of typical regions: (**a**) region A; (**b**) region B; (**c**) region C; (**d**) region D.

We then counted the proportion of each land cover type at 99%, 95%, and 90% percentile SD (Table 6). At the 99% percentile SD level, evergreen needleleaf forest, woody savannas, and mixed forest have the highest proportion with 32.87%, 16.71%, and 11%, respectively. At 95% and 90% percentile SD levels, evergreen needleleaf forest, woody savanna, and savanna have the highest proportion. Thus, from the perspective of standard deviation, the LAI discrepancy can attribute to evergreen needleleaf forest, savannas, and mixed forest.

**Table 6.** Pixel proportion of different biome types at three standard deviation percentiles.

| Biome Type | 99% Percentile | 95% Percentile | 90% Percentile |
|---|---|---|---|
| Evergreen needleleaf forest | 32.87 | 21.7 | 16.85 |
| Evergreen broadleaf forest | 4.95 | 4.64 | 4.02 |
| Deciduous needleleaf forest | 0.00 | 0.01 | 0.02 |
| Deciduous broadleaf forest | 9.24 | 4.48 | 3.46 |
| Mixed forest | 11.00 | 7.50 | 6.75 |
| Closed shrubland | 2.70 | 6.02 | 7.57 |
| Open shrubland | 5.11 | 5.13 | 5.90 |
| Woody savannas | 16.71 | 18.42 | 17.65 |
| Savannas | 9.10 | 15.44 | 16.26 |
| Grassland | 5.99 | 9.02 | 10.79 |
| Permanent wetland | 0.05 | 0.07 | 0.09 |
| Cropland | 1.61 | 6.50 | 9.44 |
| Urban and built-up | 0.10 | 0.16 | 0.19 |
| Cropland/natural vegetation mosaic | 0.08 | 0.38 | 0.45 |
| Snow/ice | 0.01 | 0.01 | 0.01 |
| Barren | 0.26 | 0.19 | 0.18 |
| Water bodies | 0.22 | 0.35 | 0.38 |

Similarly, we counted the proportion of each climate type at three percentile SD levels (Table 7). At 99% and 95% percentile SD levels, temperate hot summer/no dry season, temperate warm summer/dry winter, and temperate dry hot summer climate types are the top three, and at 90% percentile SD level, temperate dry hot summer, temperate warm summer/dry winter and cold dry winter/warm summer climate types have the highest proportion.

**Table 7.** Pixel proportion of different climate types at three standard deviation percentiles.

| Climate Type | 99% Percentile | 95% Percentile | 90% Percentile |
|---|---|---|---|
| Tropical zone monsoon | 0.33 | 0.65 | 1.03 |
| Tropical zone savannah | 1.47 | 1.98 | 2.87 |
| Arid zone cold desert | 0.28 | 0.21 | 0.29 |
| Arid zone hot steppe | 0.34 | 0.38 | 1.11 |
| Arid zone cold steppe | 0.67 | 0.59 | 1.15 |
| Temperate zone dry warm summer | 0 | 0 | 0.01 |
| Temperate zone dry hot summer | 21.28 | 22.93 | 45.88 |
| Temperate zone warm summer; dry winter | 27.52 | 15.54 | 20.74 |
| Temperate zone hot summer; no dry season | 34.45 | 45.71 | 7.68 |
| Temperate zone warm summer; no dry season | 4.19 | 2.72 | 3.87 |
| Cold zone dry warm summer | 0 | 0 | 0 |
| Cold zone dry cold summer | 0 | 0 | 0 |
| Cold zone dry winter; hot summer | 0 | 0.29 | 1.62 |
| Cold zone dry winter; warm summer | 7.49 | 6.44 | 9.49 |
| Cold zone dry winter; cold summer | 0.54 | 0.82 | 1.39 |
| Cold zone hot summer; no dry season | 0.05 | 0.22 | 0.43 |
| Cold zone warm summer; no dry season | 1.37 | 1.52 | 2.42 |
| Polar zone tundra | 0.01 | 0.01 | 0.02 |

### 3.4.3. Relative Standard Deviation (RSD)

Similar to SD, we also extracted 90%, 95%, and 99% percentiles of relative standard deviation as shown in Figure 16. The 99% percentile of RSD (red color) mainly occurs in southern Tibet and western Sichuan, which is almost the same as the SD 99% percentile regions (Section 3.4.2). The 95% percentile of RSD (green color) mainly occurs in northern Tibet (region D in Figure 16) and Guizhou province, and 90% percentile of RSD (blue color) mainly occurs in northern Tibet (region D in Figure 16); this region is also analyzed by a boxplot (Figure 15d). In region A, the GLOBMAP LAI is a little low whereas the MODIS LAI is a little high. What is more, the LAI values in this region are lower than 0.2, which may attribute to the high relative standard deviation.

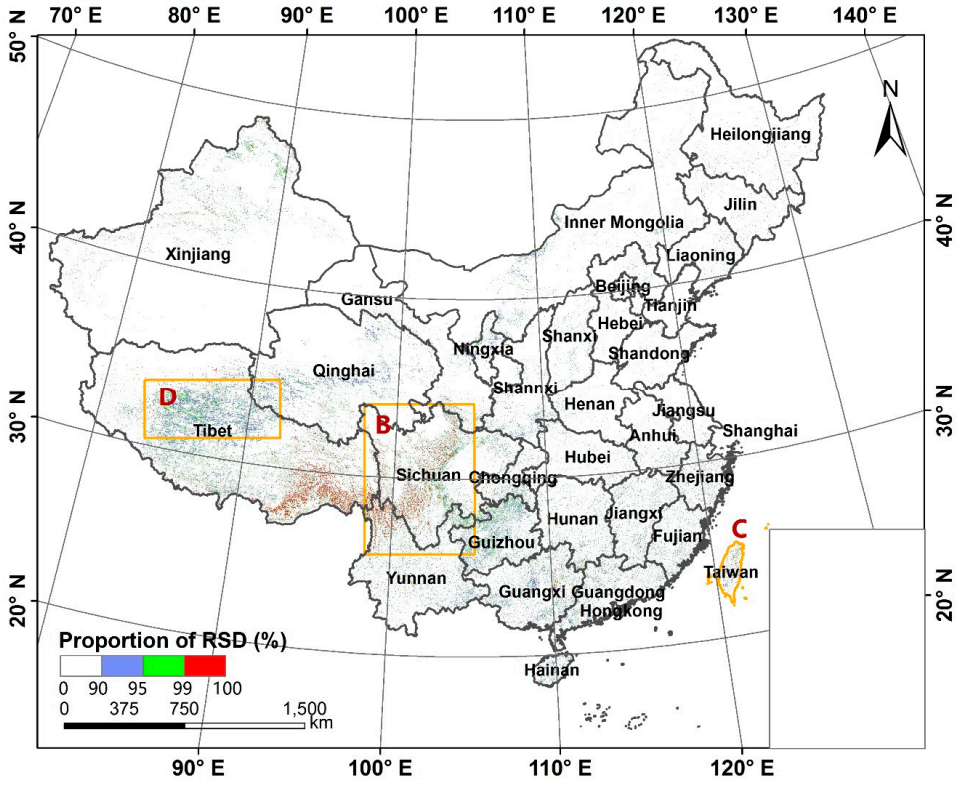


**Figure 16.** Percentile distribution of relative standard deviation of four LAI climatologies over China. Blue represents 90% percentile level, green represents 95% percentile level, and red represents 99% percentile level.

Then we counted the proportion of each land cover type at different significance levels (Table 8). At 99% and 95% percentile RSD levels, grassland, barren and evergreen needleleaf forest have the highest proportion; at the 90% percentage RSD level, grassland, cropland, barren and evergreen needleleaf forest have the highest proportion. This is generally in agreement with the RSD rankings shown in Table 4.

The results on the proportion of each climate type (Table 9) show that temperate warm summer/dry winter, cold dry winter/warm summer and temperate dry hot summer climate types are the top three at 99% percentile RSD level. Temperate warm summer/dry winter, cold dry winter/warm summer, and temperate hot summer/no dry season climate types are the top three at the 95% percentile RSD level, and temperate hot summer no dry season, cold dry winter warm summer and temperate warm summer dry winter climate types are the top three at 90% percentile RSD level.

In the LAI difference case analysis, ENF has both the highest SD and RSD among the four LAI products, while EBF and SAV have the highest SD, and SHR and GRA have the highest RSD. From the perspective of climate zones, tropical savannah, tropical monsoon, and temperate warm summer/no dry

season climate show the highest mean SD, while cold zone dry and cold summer, cold zone dry and warm summer and temperate warm summer/dry winter climate show the highest RSD. The comparison of LAI differences for each biome type indicates that GLASS, GLOBALBNU, and GLOBMAP LAI are all higher than MODIS LAI for all biome types and most of the climate types. To look at this issue more closely, the 90%, 95%, and 99% percentile of difference have been studied, and results demonstrate that ENF and woody savannas have the highest proportion of large SD, whereas ENF and grassland are responsible for large RSD; temperate dry hot summer, temperate warm summer/dry winter, and temperate hot summer/no dry season climate account for the largest SD, and temperate warm summer/dry winter and cold dry winter/warm summer climate correspond to large RSD.

**Table 8.** Pixel proportion of different biome types at three relative standard deviation percentile levels.

| Biome Type | 99% Percentile | 95% Percentile | 90% Percentile |
|---|---|---|---|
| Evergreen needleleaf forest | 20.70 | 12.12 | 9.02 |
| Evergreen broadleaf forest | 0.69 | 0.97 | 0.97 |
| Deciduous needleleaf forest | 0.08 | 0.06 | 0.05 |
| Deciduous broadleaf forest | 2.40 | 1.70 | 1.42 |
| Mixed forest | 5.96 | 3.94 | 3.21 |
| Closed shrubland | 2.34 | 4.50 | 4.80 |
| Open shrubland | 8.15 | 5.45 | 4.71 |
| Woody savannas | 10.70 | 7.89 | 7.03 |
| Savannas | 5.62 | 5.98 | 6.15 |
| Grassland | 23.92 | 32.17 | 36.14 |
| Permanent wetland | 0.47 | 0.87 | 0.99 |
| Cropland | 3.36 | 9.04 | 12.00 |
| Urban and built-up | 0.36 | 0.59 | 0.72 |
| Cropland/natural vegetation mosaic | 0.09 | 0.27 | 0.35 |
| Snow/ice | 1.03 | 0.54 | 0.37 |
| Barren | 12.79 | 12.52 | 10.87 |
| Water bodies | 1.35 | 1.39 | 1.21 |

**Table 9.** Pixel proportion of different climate types at three relative standard deviation percentile levels.

| Climate Type | 99% Percentile | 95% Percentile | 90% Percentile |
|---|---|---|---|
| Tropical zone monsoon | 0.04 | 0.14 | 0.21 |
| Tropical zone savannah | 0.08 | 0.27 | 0.39 |
| Arid zone cold desert | 3.79 | 4.71 | 5.17 |
| Arid zone hot steppe | 0.12 | 0.20 | 0.24 |
| Arid zone cold steppe | 6.91 | 10.09 | 11.80 |
| Temperate zone dry warm summer | 0 | 0 | 0 |
| Temperate zone dry hot summer | 9.23 | 14.39 | 15.72 |
| Temperate zone warm summer; dry winter | 37.54 | 21.12 | 15.72 |
| Temperate zone hot summer; no dry season | 8.82 | 16.56 | 18.67 |
| Temperate zone warm summer; no dry season | 3.80 | 2.27 | 1.70 |
| Cold zone dry warm summer | 0.11 | 0.05 | 0.03 |
| Cold zone dry cold summer | 0.02 | 0.01 | 0.01 |
| Cold zone dry winter; hot summer | 0.74 | 1.84 | 2.68 |
| Cold zone dry winter; warm summer | 20.67 | 18.10 | 16.16 |
| Cold zone dry winter; cold summer | 4.70 | 5.04 | 5.03 |
| Cold zone hot summer; no dry season | 0.11 | 0.14 | 0.15 |
| Cold zone warm summer; no dry season | 1.70 | 1.21 | 1.00 |
| Polar zone tundra | 1.62 | 3.85 | 5.31 |

## 4. Conclusions

This work evaluated four LAI products, GLASS, GLOBALBNU, GLOBMAP, and MODIS, over China using direct and indirect methods. Reference data from OLIVE platform were used for direct validation, and results show that GLASS performed best, with the highest $R^2$ (0.94) and lowest RMSE

(0.61), while MODIS performed worst, and GLOBALBNU and GLOBMAP performed moderately. This indicates that the three improved LAI products all show improvement in LAI accuracy over China.

The comparison among the four LAI products revealed that the spatial pattern of all the products agrees well with each other. The spatial correlation indicates four pairs of the products have a strong correlation ($R^2 > 0.72$), while two pairs shows moderate correlation. Compared with MODIS, the spatial correlation ranks as: GLOBALBNU > GLASS > GLOBMAP; this can be easily explained by their LAI retrieval algorithm. LAI difference analysis shows that for all types of biome and for most of the climate zones, GLASS, GLOBALBNU, and GLOBMAP LAI are higher than MODIS. Significant analysis illustrates evergreen needleleaf forest (ENF) and woody savannas (SAV) mainly correspond to large LAI SD, while evergreen needleleaf forest (ENF) and grassland (GRA) are more responsible for RSD. In view of biome types, the value of SD, ranging from 0.17 to 0.75, is partially dependent on the land cover type, i.e., biomes with large LAI have large SD. However, the RSD for all biomes is on the order of 0.3, indicating a typical 30% uncertainty for LAI products. From the perspective of climate types, temperate dry hot summer, temperate warm summer/dry winter and temperate hot summer/no dry season climate types are mainly responsible for large SD, while temperate warm summer/dry winter and cold dry winter/warm summer climate types mainly correspond to large RSD. For different climate types, the value of SD ranges from 0.05 to 0.8. However, the RSD of most climate types is on the order of 0.3, in line with the findings from biome types. Therefore, the comparison results indicate there is a typical 30% uncertainty for the four LAI products.

Our results could benefit researchers for LAI product selection and uncertainty quantification and could also provide clues for data producers to further improve their datasets. Moreover, the uncertainties quantified by this comparison could benefit researchers who include LAI as an input parameter. For instance, our results could contribute to the error matrix development in the data assimilation system developed by Huang et al. [8]. In this study, due to the page limit, we mainly focus on the spatial patterns of four LAI climatologies and annual means. In the future, we will compare the temporal variations and trends of these four LAI products, which could contribute to research related to phenology and global change. Meanwhile, there is a need to supplement more field measurements of LAI and more accurate reference maps over mainland China.

**Acknowledgments:** This work was jointly supported by the National Basic Research Program of China (No. 2015CB953703), the National Key Research and Development Program of China (2017YFA0603703), and the National Natural Science Foundation of China (91537210 & 91747101). The four LAI products were provided by the Center for Global Change Data Processing and Analysis at Beijing Normal University (BNU), the Land–Atmosphere Interaction research group at BNU, Ronggao Liu's group at the Institute of Geographic Sciences and Natural Resources Research of the Chinese Academy of Sciences (CAS), and Level 1 and Atmosphere Archive and Distribution System of National Aeronautics and Space Administration (NASA). The land cover map was provided by the Cold and Arid Regions Environmental and Engineering Research Institute, CAS. The computation of this work was supported by Tsinghua National Laboratory for Information Science and Technology. The authors also acknowledge Pauline Lovell and Arthur Cracknell for their kind help and comments on this paper.

**Author Contributions:** All authors made great contributions to this study. Hui Lu conceived and designed this study. Xinlu Li and Hui Lu performed the experiments. Xinlu Li, Hui Lu, Kun Yang, and Le Yu wrote the manuscript.

**Conflicts of Interest:** The authors declare no conflict of interest.

## References

1. Chen, J.M.; Black, T.A. Defining leaf area index for non-flat leaves. *Plant Cell Environ.* **1992**, *15*, 421–429. [CrossRef]
2. Mahowald, N.; Lo, F.; Zheng, Y.; Harrison, L.; Funk, C.; Lombardozzi, D.; Goodale, C. Projections of leaf area index in earth system models. *Earth Syst. Dyn.* **2016**, *7*, 211–229. [CrossRef]
3. Anav, A.; Murray-Tortarolo, G.; Friedlingstein, P.; Sitch, S.; Piao, S.; Zhu, Z. Evaluation of land surface models in reproducing satellite Derived leaf area index over the high-latitude northern hemisphere. Part II: Earth system models. *Remote Sens.* **2013**, *5*, 3637–3661. [CrossRef]

4. Jarlan, L.; Balsamo, G.; Lafont, S.; Beljaars, A.; Calvet, J.C.; Mougin, E. Analysis of leaf area index in the ECMWF land surface model and impact on latent heat and carbon fluxes: Application to West Africa. *J. Geophys. Res.* **2008**, *113*, D24117. [CrossRef]
5. Lu, H.; Yang, K.; Koike, T.; Zhao, L.; Qin, J. An Improvement of the Radiative Transfer Model Component of a Land Data Assimilation System and Its Validation on Different Land Characteristics. *Remote Sens.* **2015**, *7*, 6358–6379. [CrossRef]
6. Liou, Y.A.; England, A.W. A land surface process/radiobrightness model with coupled heat and moisture transport for prairie grassland. *IEEE Trans. Geosci. Remote Sens.* **1999**, *37*, 1848–1858. [CrossRef]
7. Liou, Y.A.; Kar, S.K. Evapotranspiration Estimation with Remote Sensing and Various Surface Energy Balance Algorithms—A Review. *Energies* **2014**, *7*, 2821–2849. [CrossRef]
8. Huang, J.; Sedano, F.; Huang, Y.; Ma, H.; Li, X.; Liang, S.; Tian, L.; Zhang, X.; Fan, J.; Wu, W. Assimilating a synthetic Kalman filter leaf area index series into the WOFOST model to improve regional winter wheat yield estimation. *Agric. For. Mettorol.* **2016**, *216*, 188–202. [CrossRef]
9. Morisette, J.T.; Baret, F.; Privette, J.L.; Myneni, R.B.; Nickeson, J.E.; Garrigues, S.; Shabanov, N.V.; Weiss, M.; Fernandes, R.A.; Lebla, S.G.; et al. Validation of global moderate-resolution LAI products: A framework proposed within the CEOS land product validation subgroup. *IEEE Trans. Geosci. Remote Sens.* **2006**, *44*, 1804–1817. [CrossRef]
10. Liang, S.; Zhao, X.; Liu, S.; Yuan, W.; Cheng, X.; Xiao, Z.; Zhang, X.; Liu, Q.; Cheng, J.; Tang, H.; et al. A long-term Global LAnd Surface Satellite (GLASS) data-set for environmental studies. *Int. J. Digit. Earth* **2013**, *6*, 5–33. [CrossRef]
11. Baret, F.; Weiss, M.; Lacaze, R.; Camacho, F.; Makhmara, H.; Pacholcyzk, P.; Smets, B. GEOV1: LAI, FAPAR Essential Climate Variables and FCOVER global time series capitalizing over existing products. Part1: Principles of development and production. *Remote Sens. Environ.* **2013**, *137*, 299–309. [CrossRef]
12. Myneni, R.B.; Hoffman, S.; Knyazikhin, Y.; Privette, J.L.; Glassy, J.; Tian, Y.; Wang, Y.; Song, X.; Zhang, Y.; Smith, G.R.; et al. Global products of vegetation leaf area and fraction absorbed PAR from year one of MODIS data. *Remote Sens. Environ.* **2002**, *83*, 214–231. [CrossRef]
13. Yuan, H.; Dai, Y.J.; Xiao, Z.Q.; Ji, D.; Shangguan, W. Reprocessing the MODIS Leaf Area Index products for land surface and climate modelling. *Remote Sens. Environ.* **2011**, *115*, 1171–1187. [CrossRef]
14. Liu, Y.; Liu, R.; Chen, J.M. Retrospective retrieval of long-term consistent global leaf area index (1981–2011) from combined AVHRR and MODIS data. *J. Geophys. Res.* **2012**, *117*. [CrossRef]
15. Baret, F.; Hagolle, O.; Geiger, B.; Bicheron, P.; Miras, B.; Huc, M.; Berthelot, B.; Niño, F.; Weiss, M.; Samain, O.; et al. LAI, fAPAR and fCover CYCLOPES global products derived from VEGETATION: Part 1: Principles of the algorithm. *Remote Sens. Environ.* **2007**, *110*, 275–286. [CrossRef]
16. Deng, F.; Chen, J.M.; Plummer, S. Algorithm for global leaf area index retrieval using satellite imagery. *IEEE Trans. Geosci. Remote Sens.* **2006**, *44*, 2219–2229. [CrossRef]
17. Masson, V.; Champeaux, J.L.; Chauvin, F.; Meriguet, C.; Lacaze, R. A Global Database of Land Surface Parameters at 1-km Resolution in Meteorological and Climate Models. *J. Clim.* **2003**, *16*, 1261–1282. [CrossRef]
18. Fernandes, R.A.; Butson, C.; Leblanc, S. Landsat-5 TM and Landsat-7ETM+ based accuracy assessment of leaf area index products for Canada derived from SPOT4/VGT data. *Can. J. Remote Sens.* **2003**, *29*, 241–258. [CrossRef]
19. Fang, H.; Jiang, C.; Li, W.; Wei, S.; Baret, F.; Garcia-Haro, J.; Liang, S.; Liu, R.; Pinty, B.; Xiao, Z.; et al. Characterization and intercomparison of global moderate resolution leaf area index (LAI) products: Analysis of climatologies and theoretical uncertainties. *J. Geophys. Res. Biogeosci.* **2013**, *118*, 529–548. [CrossRef]
20. Xua, B.D.; Li, J.; Liu, Q.H.; Zeng, Y.; Yin, G. A methodology to estimate representativeness of LAI station observation for validation: A case study with Chinese Ecosystem Research Network (CERN) in situ data. *SPIE Asia Pac. Remote Sens.* **2015**, *9260*. [CrossRef]
21. Justice, C.; Belward, A.; Morisette, J.; Lewis, P.; Privette, J.; Baret, F. Developments in the 'validation' of satellite sensor products for the study of the land surface. *Int. J. Remote Sens.* **2000**, *21*, 3383–3390. [CrossRef]
22. Garrigues, S.; Lacaze, R.; Baret, F.; Morisette, J.T.; Weiss, M.; Nickeson, J.E.; Fernandes, R.; Plummer, S.; Shabanov, N.V.; Myneni, R.B.; et al. Validation and intercomparison of global Leaf Area Index products derived from remote sensing data. *J. Geophys. Res.* **2008**, *113*, G02028. [CrossRef]

23. Weiss, M.; Baret, F.; Block, T.; Koetz, B.; Burini, A.; Scholze, B.; Lecharpentier, P.; Brockmann, C.; Fernandes, R.; Plummer, S.; et al. On Line Validation Exercise (OLIVE): A Web Based Service for the Validation of Medium Resolution Land Products. Application to FAPAR Products. *Remote Sens.* **2014**, *6*, 4190–4216. [CrossRef]
24. Baret, F.; Morissette, J.T.; Fernandes, R.A.; Champeaux, J.L.; Myneni, R.B.; Chen, J.; Plummer, S.; Weiss, M.; Bacour, C.; Garrigues, S.; et al. Evaluation of the representativeness of networks of sites for the global validation and inter-comparison of land biophysical products: Proposition of the CEOS-BELMANIP. *IEEE Trans. Geosci. Remote Sens.* **2006**, *44*, 1794–1803. [CrossRef]
25. Zhu, L.; Chen, J.M.; Tang, S.H.; Li, G.; Guo, Z. Inter-Comparison and Validation of the FY-3A/MERSI LAI Product Over Mainland China. *IEEE Trans. Geosci. Remote Sens.* **2014**, *7*, 458–468. [CrossRef]
26. Martin, K.; Pavel, P.; Jan, D. Inter-Comparison and Evaluation of the Global LAI Product (LAI3g) and the Regional LAI Product (GGRS-LAI) over the Area of Kazakhstan. *Remote Sens.* **2015**, *7*, 3760–3782.
27. Knyazikhin, Y.; Martonchik, J.V.; Myneni, R.B.; Diner, D.J.; Running, S.W. Synergistic algorithm for estimating vegetation canopy leaf area index and fraction of absorbed photosynthetically active radiation from MODIS and MISR data. *J. Geophys. Res.* **1998**, *103*, 257–275. [CrossRef]
28. Xiao, Z.; Liang, S.; Wang, J.; Xiang, Y.; Zhao, X.; Song, J. Long-Time-Series Global Land Surface Satellite Leaf Area Index Product Derived From MODIS and AVHRR Surface Reflectance. *IEEE Trans. Geosci. Remote Sens.* **2016**, *54*, 5301–5318. [CrossRef]
29. Xiao, Z.; Liang, S.; Wang, J.; Chen, P.; Yin, X.; Zhang, L.; Song, J. Use of General Regression Neural Networks for Generating the GLASS Leaf Area Index Product From Time-Series MODIS Surface Reflectance. *IEEE Trans. Geosci. Remote Sens.* **2014**, *52*, 209–223. [CrossRef]
30. Fang, H.; Liang, S.; Townshend, J.R.; Dickinson, R.E. Spatially and temporally continuous LAI data sets based on an integrated filtering method: Examples from North America. *Remote Sens. Environ.* **2008**, *112*, 75–93. [CrossRef]
31. Jiao, T.; Liu, R.G.; Liu, Y.; Pisek, J.; Chen, J.M. Mapping global seasonal forestbackground reflectivity with Multi-angleImaging Spectroradiometer data. *J. Geophys. Res. Biogeosci.* **2014**, *119*. [CrossRef]
32. Ran, Y.H.; Li, X.; Lu, L. Evaluation of four remote sensing based land cover products over China. *Int. J. Remote Sens.* **2010**, *31*, 391–401. [CrossRef]
33. Peel, M.C.; Finlayson, B.L.; Mcmahon, T.A. Updated world map of the Köppen-Geiger climate classification. *Hydrol. Earth Syst. Sci.* **2007**, *11*, 259–263. [CrossRef]
34. Chen, J.M.; Govind, A.; Sonnentag, O.; Zhang, Y.; Barr, A.; Amiro, B. Leaf area index measurements at Fluxnet Canada forest sites. *Agric. For. Meteorol.* **2006**, *14*, 257–268. [CrossRef]
35. Chen, J.M.; Rich, P.; Gower, S.T.; Norman, J.M.; Plummer, S. Leaf area index of boreal forests: Theory, techniques and measurements. *J. Geophys. Res.* **1997**, *29*, 429–443. [CrossRef]
36. Tang, H.R.; Yu, K.; Hagolle, O.; Jiang, K.; Geng, X.; Zhao, Y. A cloud detection method based on a time series of MODIS surface reflectance images. *Int. J. Digit. Earth* **2013**, *6*, 157–171. [CrossRef]
37. Pisek, J.; Govind, A.; Arndt, S.K.; Hocking, D.; Wardlaw, T.J.; Fang, H.; Matteucci, G.; Longdoz, B. Intercomparison of clumping index estimates from POLDER, MODIS, and MISR satellite data over reference sites. *ISPRS J. Photogram. Remote Sens.* **2015**, *101*, 47–56. [CrossRef]
38. Pisek, J.; Chen, J.M.; Lacaze, R.; Sonnentag, O.; Alikas, K. Expanding global mapping of the foliage clumping index with multi-angular POLDER three measurements: Evaluation and topographic compensation. *ISPRS J. Photogram. Remote Sens.* **2010**, *65*, 341–346. [CrossRef]
39. Chen, J.M.; Menges, C.H.; Leblanc, S.G. Global mapping of foliage clumping index using mutli-angular satellite data. *Remote Sen. Environ.* **2005**, *97*, 447–457. [CrossRef]